Available online at www.sciencedirect.com
SCIENCE DIRECT
Journal of Catalysis 236 (2005) 205–220
JOURNAL OF CATALYSIS
www.elsevier.com/locate/jcat

Novel Fe–Mn–Zn–Ti–O mixed-metal oxides for the low-temperature removal of H_2S from gas streams in the presence of H_2, CO_2, and H_2O

K. Polychronopoulou [a], F. Cabello Galisteo [b], M. López Granados [b], J.L.G. Fierro [b], T. Bakas [c], A.M. Efstathiou [a,*]

[a] *Department of Chemistry, University of Cyprus, P.O. Box 20537, CY 1678 Nicosia, Cyprus*
[b] *Instituto de Catálisis y Petroleoquimica, CSIC, C/Marie Curie 2, Cantoblanco, 28049 Madrid, Spain*
[c] *Physics Department, University of Ioannina, P.O. Box 1186, 45110, Greece*

Received 4 August 2005; revised 29 September 2005; accepted 1 October 2005

Available online 28 October 2005

Abstract

The efficiency of Fe–Mn–Zn–Ti–O mixed-metal oxides of varying composition prepared by sol–gel methods toward removal of H_2S from a gas mixture containing 0.06 vol% H_2S, 25 vol% H_2, 7.5 vol% CO_2, and 1–3 vol% H_2O was studied in the 25–100 °C range. In particular, the effects of the Fe/Mn molar ratio in the Fe–Mn–Zn–Ti–O solids on the H_2S uptake and regeneration performance of the solids were studied. The nominal chemical composition (metal mol%) of the Fe–Mn–Zn–Ti–O solids was found to strongly influence the chemical composition, particle size, and morphology of the crystal phases formed. It was found that the 5 Fe–15 Mn–40 Zn–40 Ti–O mixed-metal oxide provides the highest H_2S uptake as fresh and after regeneration in 20% O_2/He gas mixture in the 500–750 °C range compared with the other solids investigated. It was also found that 5 Fe–15 Mn–40 Zn–40 Ti–O exhibits higher H_2S uptake than a commercial Ni-based H_2S adsorbent in the 25–50 °C range. In particular, a three times greater H_2S uptake at 25 °C compared with that on the commercial adsorbent was found. The effectiveness of the regeneration procedure of 5 Fe–15 Mn–40 Zn–40 Ti–O solid after complete sulfidation was found to be in the 48–82% range, depending on the sulfidation temperature and regeneration conditions applied. A detailed characterization of the fresh, sulfided, and regenerated 5 Fe–15 Mn–40 Zn–40 Ti–O and 20 Fe–40 Zn–40 Ti–O solids, which exhibited the best and worst H_2S uptake performance, respectively, using BET, XRD, Raman, XPS, and Mössbauer techniques revealed important information on the sulfidation mechanism. The present work provides new fundamental knowledge that could trigger further research efforts toward the development of alternative mixed metal oxides not based on toxic chromia (Cr_2O_3–Fe_2O_3/α-Al_2O_3), which is used today in several industrial plants for the catalytic oxidation of H_2S (Claus process).

Keywords: H_2S removal; Fe-based H_2S adsorbents; Mixed metal oxides; Zinc ferrite spinels; Sulfidation; Adsorbent regeneration; H_2-TPR; Mössbauer; Raman; XPS

1. Introduction

The removal of H_2S from a gas stream can be accomplished by adsorption onto a solid surface [1,2], catalytic oxidation [3–5], and absorption by a liquid solution (amine/alkaloamine) [5]. Various solid materials have been developed to remove H_2S from a number of industrial gas effluent streams. Most of the work carried out to date on the development of H_2S solid adsorbents has been focused on materials suitable at temperatures >300 °C. Among the most studied solid materials for the removal of H_2S from a "coal-gas" are Fe- and Ca-containing materials, because of their high reactivity and low cost [6,7]. However, due to the fact that "coal-gas" contains a large fraction of H_2 and a high CO/CO_2 ratio, these materials have some drawbacks. For example, Fe_3O_4 is reduced to FeO and Fe, whereas the formation of Fe_3C reduces the sulfur uptake of the solid [6–8]. Moreover, regenerating the sulfided Ca-containing solids is very difficult. Lew et al. [9] have shown that ZnO is more attractive than iron oxide because of its more favorable sulfidation thermodynamics. On the other hand, ZnO has much slower sulfidation kinetics than iron oxide. A major limitation

* Corresponding author. Fax: +357 22 892801.
E-mail address: efstath@ucy.ac.cy (A.M. Efstathiou).

0021-9517/$ – see front matter
doi:10.1016/j.jcat.2005.10.001

of ZnO-based adsorbents for hot-gas cleaning is their loss due to reduction of ZnO to volatile elemental zinc.

Mixed metal oxides, such as Cu–Mn–O, Cu–Fe–O, Cu–Mo–O, Zn–V–O, Zn–Ti–O, Zn–Fe–Ti–O, and Zn–Fe–V–O, have been studied as H_2S adsorbent materials [10–13]. Their reactivity and regeneration ability are improved when deposited on a suitable support. $ZnFe_2O_4$ mixed-metal oxide was also found to be a good H_2S adsorbent in the 500–700 °C range [14,15]. Kobayashi et al. [16,17] studied zinc ferrite–silicon dioxide composites as high-temperature fuel gas desulfurization adsorbents. Sulfidation of zinc ferrite in the reducing environment yielded wurtzite, zinc blende, and iron sulfides in the presence of 500 ppm of H_2S.

Little research work has been carried out on the development and characterization of solid materials for low-temperature removal of H_2S [18–28]. Carnes and Klabunde [22] studied nanocrystalline metal oxides prepared by sol–gel methods. At low temperatures (25–100 °C), the activity order was ZnO > CaO > $Al_2O_3 \gg$ MgO. Davidson et al. [19] reported on the adsorption of H_2S on ZnO in the 25–45 °C range, where about 40% conversion of H_2S was observed. Sasaoka et al. [23] studied the adsorption of H_2S on ZnO in the presence of CO, CO_2, and H_2O and found that CO inhibits sulfidation reaction due to its competitive adsorption with H_2S for the same active sites, whereas H_2O inhibits the reaction due to promotion of the reaction with ZnS to form H_2S and ZnO. Baird et al. [24] have found that mineral feroxyhyte is an efficient adsorbent of H_2S at room temperature due to its high surface area and the presence of the Fe^{3+}/Fe^{2+} redox couple. In another study, Baird et al. [18] found that reaction of H_2S with ZnO doped with first-row transition metals was restricted to about 0.6 surface monolayers. The main role of the transition metal oxide was to increase the total surface area available for reaction with H_2S. Baird et al. [25] studied Co–Zn–Al–O mixed-metal oxides as H_2S adsorbents at 28 °C. A comparison of H_2S uptake with Co–Zn–O uptake suggested that the presence of aluminum ions in the mixed-oxide matrix gave rise to an increased surface area, but not to H_2S uptake. Other H_2S adsorbent materials that have been investigated include activated carbons [26,27], the surface acid chemistry of which has been shown to play an important role.

The present work concerns the development of novel Fe–Mn–Zn–Ti–O mixed-metal oxides prepared by sol–gel methods and tested for the first time toward low-temperature removal of H_2S from a gas mixture containing H_2, CO_2, and H_2O. The following parameters have been investigated with respect to their effects on the H_2S uptake performance of the solids investigated: mixed-metal oxide composition, adsorption temperature, temperature of adsorbent regeneration in 20% O_2/He, time of regeneration in 20% O_2/He, and presence of water in the feed stream. A commercial Ni-based catalyst was also investigated for a critical comparison. A detailed characterization of some of the fresh, sulfided, and regenerated Fe–Mn–Zn–Ti–O solids using BET, XRD, Raman, XPS, and Mössbauer techniques has revealed important information on the sulfidation mechanism.

The selective catalytic oxidation of H_2S to elemental sulfur (Claus reaction) is an industrial practice that makes use of α-Al_2O_3-supported iron and chromium oxides [29,30]. Continuing research is being conducted into the development of new materials for this important catalytic reaction, excluding the use of Cr_2O_3 because of its severe toxicity. Despite numerous investigations into the mechanism of this reaction over different metal oxides [31,32], a detailed mechanism based on which further significant catalyst developments would be expected has not yet been established. The selection of a better catalyst for the Claus reaction is still based on a modification of the surface acid/base properties of mixed-metal oxides [32,33]. Li et al. [34] reported that Fe–Sb–O and Fe–Sn–O mixed-metal oxides are good H_2S oxidation to sulfur catalysts. The catalytic properties of these materials change significantly with their composition.

Based on the work mentioned in the previous paragraph, the results of the present work, which relate to the chemisorption and bulk chemical reaction of H_2S with new Fe–Mn–Zn–Ti–O mixed metal oxides and also to the oxidation (use of air) of the latter sulfated solids, could trigger further research into Fe–Mn–Zn–Ti–O mixed-metal oxides as important catalytic materials for the oxidation of H_2S to elemental sulfur. The present work was motivated by a European project [35] in which the gas effluent stream from a bioreactor used to reduce toxic Cr^{6+} present in waters into Cr^{3+} after using the sulfate metal-reducing bacteria (SMRB) had to be treated to remove the nondesirable H_2S gas evolved.

2. Experimental

2.1. Synthesis of H_2S solid adsorbent materials

A series of Fe–Mn–Zn–Ti–O mixed-metal oxides were prepared by the sol–gel method [36] using $Fe(NO_3)_3$, $(CH_3COO)_2Mn$, $(CH_3COO)_2Zn$, and Ti(i-OPr)$_4$ (Aldrich) as precursors of Fe, Mn, Zn and Ti, respectively. Appropriate amounts of each reagent were used to obtain a (Fe + Mn)/(Fe + Mn + Zn + Ti) molar ratio of 0.2 and Fe/Mn molar ratios of 15/5, 10/10, and 5/15 in the final product. An 20 Fe–40 Zn–40 Ti–O solid composition was also prepared. An appropriate amount of $(CH_3COO)_2Zn$ was dissolved in H_2O, and the pH of the resulting solution was adjusted in the 8.5–9.4 range by dropwise addition of ammonia solution (25% v/v). Appropriate amounts of iron nitrate, manganese acetate, and titanium isopropoxide solutions were then added, with the pH kept within the same range, until the formation of a brown gel-like product was noted. This product was then dried at 70 °C overnight in the presence of air. The dried powders were finally calcined in air at 100 °C for 1.5 h, at 150 °C for 1.5 h, at 200 °C for 2.5 h, and finally at 500 °C for 4 h before storage and further use.

A second series of Fe–Mn–Zn–Ti–O mixed-metal oxides were synthesized by means of co-hydrolysis of iron nitrate, manganese acetate, zinc acetate, and titanium isopropoxide. Appropriate amounts of each reagent were used so as to yield a (Fe + Mn)/(Fe + Mn + Zn + Ti) molar ratio of 0.1 in the final product, with Fe/Mn molar ratios of 7/3 and 5/5.

2.2. Characterization of H_2S solid adsorbent materials

2.2.1. Surface area measurements

The specific surface area (BET, m^2/g) of solid adsorbents was checked by N_2 adsorption at 77 K (Micromeritics 2100E Accusorb). Before any measurements were taken, the samples were outgassed at 400 °C under vacuum ($P \sim 1.3 \times 10^{-3}$ mbar) overnight. The BET areas of fresh H_2S adsorbents, as well as those after adsorption from a $H_2S/H_2/CO_2$/He gas mixture and regeneration in 20% O_2/He gas mixture at 500 or 750 °C, were also measured.

2.2.2. XRD analyses

The crystal structure of the sol–gel-prepared solids was studied by XRD (Shimazdu 6000 Series, Cu-K_α radiation ($\lambda = 1.5418$ Å)). The crystal structures of the solid adsorbents with the best and worst performance toward H_2S removal were also determined after sulfidation and regeneration conditions.

2.2.3. SEM studies

The particle size and morphology of the solids (fresh, after exposure to sulfidation and regeneration conditions) were examined through a JEOL JSM 5200 scanning electron microscope (25 kV). Powdered specimens were spread on the SEM slabs and sputtered with gold.

2.2.4. Raman studies

Raman spectra were recorded with a Renishaw 1000 spectrophotometer equipped with a cooled (−73 °C) CCD detector and a holographic Notch filter to remove the elastic scattering. Samples were excited with a 514-nm Ar line. Spectra acquisition consisted of 5 scans of 60-s duration. All samples were pretreated in dry air at 250 °C (100 NmL/min, 30 min) in an in situ cell (Linkam, TS-1500) before the spectra were recorded at 200 °C under dry air flow.

2.2.5. X-Ray photoelectron spectroscopy studies

The surface chemical composition (at%) of certain H_2S solid adsorbents (fresh, after sulfidation and regeneration) was studied by X-ray photoelectron spectroscopy (XPS). The sample in powder form was pressed firmly into a carved stainless steel holder so that it could be introduced into the ultra-high-vacuum (UHV) chamber. The UHV system (base pressure 8×10^{-10} mbar) consisted of a fast entry assembly and the preparation and analyses chambers. The latter was equipped with a hemispherical analyzer (SPECS LH-10) and a twin-anode X-ray gun.

2.2.6. H_2 temperature-programmed reduction studies

H_2 temperature-programmed reduction (TPR) experiments were conducted by passing a 2% H_2/He gas mixture (30 NmL/min) over 0.2 g of the precalcined solid at a temperature ramp of 30 °C/min. The hydrogen concentration as a function of temperature was monitored using an on line mass spectrometer (Omnistar, Balzers). The mass numbers (m/z) 2, 18, and 32 were used for H_2, H_2O, and O_2, respectively. Based on material balances, the rate of hydrogen consumption (μmol/(g min)) versus temperature was estimated. The redox behavior of the 5 Fe–15 Mn–40 Zn–40 Ti–O solid was also studied under three consecutive TPR runs.

2.2.7. Temperature-programmed desorption studies

Temperature-programmed desorption (TPD) of NH_3 and CO_2 experiments were conducted to study the surface acidity and basicity, respectively, of the H_2S solid adsorbents. The amount of sample used was 0.2 g, the heating rate was 30 °C/min, and the He gas flow rate was 30 NmL/min. The mass numbers (m/z) 15, 30, and 44 were used for NH_3, NO, and N_2O, respectively (NH_3-TPD), and 28 and 44 were used for CO and CO_2, respectively (CO_2-TPD). Ammonia and carbon dioxide chemisorption was conducted at room temperature. Before NH_3 and CO_2 chemisorption occurred, all samples were pretreated in a 20% O_2/He gas mixture at 500 °C for 2 h. NH_3-TPD and CO_2-TPD experiments were also conducted after adsorption of H_2S from a $H_2S/H_2/CO_2$/He gas mixture and after regeneration of the sulfided solid.

2.2.8. Mössbauer studies

Mössbauer measurements were carried out with a conventional constant acceleration spectrometer equipped with a ^{57}Co(Rh) source (calibrated with α-Fe). Isomer shift values are reported relative to this. The spectra recorded at ambient temperature were fitted by a least squares minimization procedure assuming Lorentzian line shapes.

2.2.9. Transient H_2S uptake studies

The gas flow system for conducting transient adsorption of H_2S experiments, the microreactor, and the analysis system have been described elsewhere [37]. H_2S uptake of the solids was determined by transient isothermal adsorption from a 0.06% H_2S/7.5% CO_2/25% H_2/He gas mixture at 25–100 °C. Before adsorption, the catalyst was pretreated in 20% O_2/He at 500 °C for 2 h, then purged in He at 500 °C for 30 min. The reactor was then cooled in He to the adsorption temperature. The amount of solid adsorbent used was 5 mg diluted in 45 mg of SiO_2, whereas the total flow rate was 30 NmL/min. Chemical analysis of the gas effluent stream of the reactor during transient adsorption was done with an on-line quadrupole mass spectrometer (Omnistar, Balzers) equipped with a fast-response inlet capillary/leak valve (SVI 050, Balzers) and data acquisition systems. The mass numbers (m/z) 34, 64, 44, 18, and 32 were used for H_2S, SO_2, CO_2, H_2O, and O_2, respectively.

3. Results and discussion

3.1. Catalyst characterization

3.1.1. BET surface area measurements

For the fresh Fe–Mn–Zn–Ti–O series (Fe + Mn = 20 mol%) of mixed-metal oxides, the BET surface area was found to decrease with increasing Fe content in the solid (Table 1). A 47% decrease in the BET area of the 5 Fe–15 Mn–40 Zn–40 Ti–O solid was found after sulfidation at 25 °C and regeneration at 500 °C. The surface area of the 20 Fe–40 Zn–40 Ti–O solid

Table 1
BET surface areas (m^2/g) of various mixed metal oxides obtained after different gas treatments

Mixed metal oxide	BET (m^2/g)	
	Fresh[a]	Used[b]
5 Fe–15 Mn–40 Zn–40 Ti–O	107.4	56.0
10 Fe–10 Mn–40 Zn–40 Ti–O	75.0	39.0
15 Fe–5 Mn–40 Zn–40 Ti–O	46.7	25.0
20 Fe–40 Zn–40 Ti–O	1.7	2.1
5 Fe–5 Mn–45 Zn–45 Ti–O	144.5	72.0
7 Fe–3 Mn–45 Zn–45 Ti–O	112.6	60.0

[a] After calcination in 20% O_2/He at 500 °C for 4 h.
[b] After sulfidation (0.06% H_2S/25% H_2/7.5% CO_2/He) at 25 °C for 0.5 h followed by regeneration in 20% O_2/He at 500 °C for 4 h.

($1.7\ m^2/g$) was slightly increased after sulfidation but still remained at the same low level compared with that of the fresh solid. The BET surface area of the solids with a total content of 10 mol% (Fe + Mn) was greater than that of the solids with a total content of 20 mol%. This is due to the higher concentration of Zn^{2+} used in the former solids. It has been reported [38] that the smaller Zn^{2+} cation (in comparison with the larger Mn^{2+} one) causes shrinkage of the Mn–Zn ferrite oxide lattice, leading to increased BET surface area. Akyurtlu and Akyurtlu [39] reported the synthesis of zinc ferrite (25.8 wt% Zn and 44 wt% Fe) with a BET area of $3.6\ m^2/g$ after calcination at 600 °C. Vanadium-doped zinc ferrites also exhibited low BET surface areas (1.0–3.0 m^2/g) [33]. Kim et al. [40] reported the synthesis of Ni-doped zinc ferrites with a BET surface area of $77.6\ m^2/g$. Baldi et al. [41] reported the synthesis of Fe–Mn–O mixed-metal oxides (50:50 ratio of Fe_2O_3:Mn_2O_3) with a BET area of $11\ m^2/g$. Table 1 gives the surface areas of all H_2S solid adsorbents synthesized in the present work (fresh) and those after used in H_2S adsorption and regeneration studies.

3.1.2. X-Ray diffraction studies

Fig. 1A(a) shows XRD patterns of the 5 Fe–15 Mn–40 Zn–40 Ti–O solid (fresh) after calcination at 500 °C (see Section 2.1). The main crystalline phases detected were (Mn,Zn)Fe_2O_4 (1), $ZnMnO_3$ (2), and $ZnTiO_3$ (3), according to ASTM data. After exposure to the $H_2S/H_2/CO_2$/He gas mixture at 100 °C for 0.5 h (Fig. 1A(b)), the solid exhibits broader diffraction peaks with lower intensities compared with those of the fresh solid. XRD peak broadening is due to a decrease of the crystalline long-range order and is associated with decreasing crystalline domain size and/or accumulated strain [42]. A new peak of low intensity appears at 28.6° and 47.9° and is assigned to ZnS (peak 4, Fig. 1A(b)). The solid after sulfidation shows diffraction peaks shifted to lower 2θ angles compared with the fresh solid. For example, as shown in Fig. 1B, the XRD peaks at 36° and 62.7° (2θ) in the fresh sample shift to 35.5° and 62.3°, respectively, after sulfidation. This shift is another proof of the structural changes occurred during the applied sulfidation conditions. It has been reported [43] that metal sulfides formation and their effect on the oxidation of H_2S to elemental sulfur (Claus industrial process), along with structural changes in the oxidic phases of the industrially used catalysts, are important to the understanding of this catalytic chemistry mechanism.

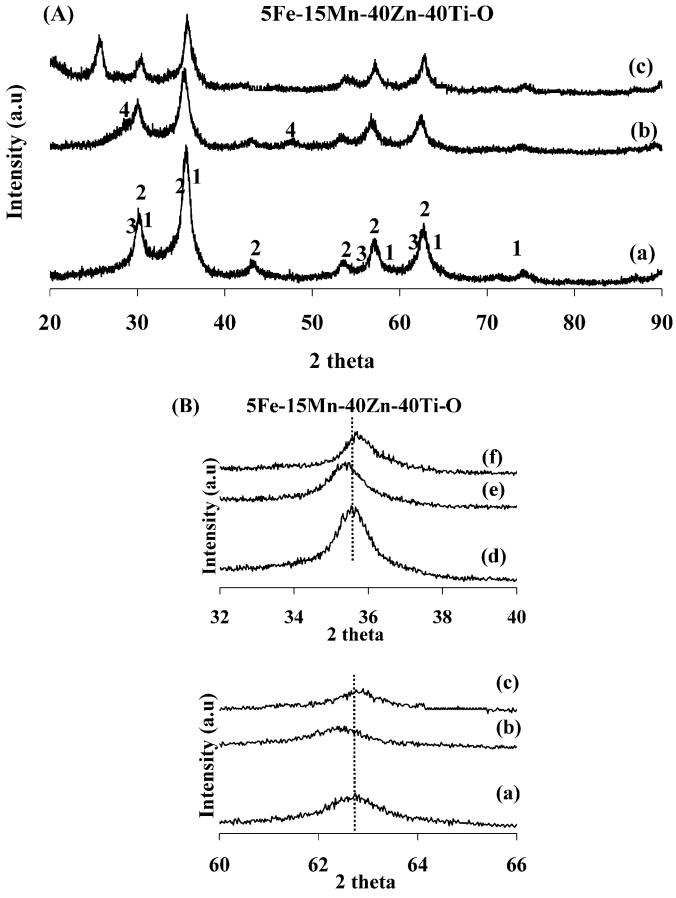

Fig. 1. (A) XRD patterns of 5 Fe–15 Mn–40 Zn–40 Ti–O solid. (a) Fresh (calcined in 20% O_2/He, 500 °C, 4 h); (b) after sulfidation ($H_2S/H_2/CO_2$/He, 100 °C, 0.5 h); (c) after sulfidation followed by regeneration (20% O_2/He, 750 °C, 10 h). (B) 2θ XRD peak shifts in the 32°–66° 2θ range. XRD peaks: (1) (Mn,Zn)Fe_2O_4; (2) $ZnMnO_3$; (3) $ZnTiO_3$; (4) ZnS; (5) MnS.

After regeneration at 750 °C for 10 h (Fig. 1A(c)), the XRD peaks at 28.9° and 48.2° that correspond to ZnS disappear, and a new peak assigned to Fe_2O_3 appears (peak 5, Fig. 1A(c)). These results indicate the efficiency of the regeneration procedure applied for the particular solid composition. Comparing the intensity of the peak at 43.5° (peak 2, $ZnMnO_3$) in the three XRD patterns of Fig. 1A demonstrates that the particular peak intensity progressively diminishes from the fresh sample to the sulfided sample and completely vanishes in the regenerated sample.

XRD studies were also conducted over the 20 Fe–40 Zn–40 Ti–O solid as fresh (Fig. 2a), after exposure to the $H_2S/H_2/CO_2$/He gas mixture at 100 °C for 0.5 h (Fig. 2b), and after regeneration at 500 °C for 4 h (Fig. 2c). The main crystalline phases detected in the fresh solid were $ZnFe_2O_4$ (1) TiO_2 (2), $ZnTiO_3$ (3), and Fe_2O_3 (5). In the case of regenerated sample (Fig. 2c), two new peaks appeared (at $2\theta = 14.1°$ and 16.9°) due to the presence of $Fe_2(SO_4)_3$ (peak 6). The presence of iron sulfate in the regenerated samples of the Fe–Mn–Zn–Ti–O series of solids was also detected by XPS studies. No characteristic peaks of MnS, FeS, and ZnS were noticed. The differences

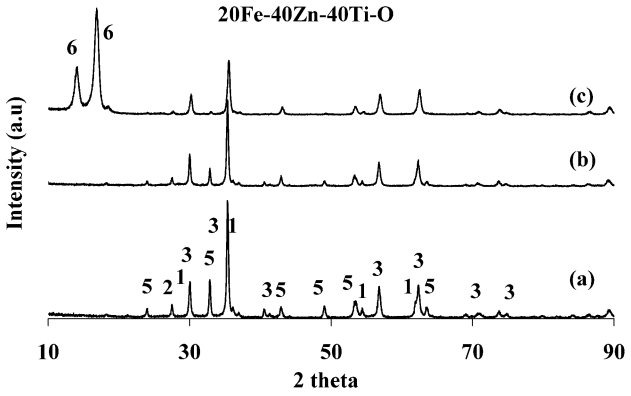

Fig. 2. XRD patterns of 20 Fe–40 Zn–40 Ti–O solid. (a) Fresh (calcined in 20% O_2/He, 500 °C, 4 h); (b) after sulfidation ($H_2S/H_2/CO_2$/He, 100 °C, 0.5 h); (c) after sulfidation followed by regeneration (20% O_2/He, 750 °C, 10 h). XRD peaks: (1) $ZnFe_2O_4$; (2) TiO_2; (3) $ZnTiO_3$; (5) Fe_2O_3; (6) $Fe_2(SO_4)_3$.

Table 2
XRD crystalline phases of various H_2S solid adsorbents prepared by the sol–gel method

Solid adsorbent[a]	Crystalline phases
5 Fe–15 Mn–40 Zn–40 Ti–O	$ZnMnO_3$, $ZnTiO_3$, $(Mn,Zn)Fe_2O_4$
10 Fe–10 Mn–40 Zn–40 Ti–O	$ZnMnO_3$, $ZnTiO_3$, $(Mn,Zn)Fe_2O_4$
15 Fe–5 Mn–40 Zn–40 Ti–O	$ZnMnO_3$, $ZnTiO_3$, $(Mn,Zn)Fe_2O_4$
20 Fe–40 Zn–40 Ti–O	$ZnTiO_3$, $ZnFe_2O_4$, Fe_2O_3, TiO_2
5 Fe–5 Mn–45 Zn–45 Ti–O	$ZnMnO_3$, $ZnTiO_3$, $(Mn,Zn)Fe_2O_4$
7 Fe–3 Mn–45 Zn–45 Ti–O	$ZnMnO_3$, $ZnTiO_3$, $(Mn,Zn)Fe_2O_4$

[a] The solids were calcined in 20% O_2/He at 500 °C for 4 h before XRD measurements were taken.

in 2θ (XRD peaks) among fresh, sulfided, and regenerated samples for the 20 Fe–40 Zn–40 Ti–O solid were smaller than those for 5 Fe–15 Mn–40 Zn–40 Ti–O. This result suggests a minor influence of the gas applied treatments on the structural changes in 20 Fe–40 Zn–40 Ti–O solid. Table 2 lists the main crystalline phases detected in all fresh solid adsorbents tested for H_2S uptake efficiency.

3.1.3. SEM studies

Fig. 3 presents SEM micrographs of the 5 Fe–15 Mn–40 Zn–40 Ti–O fresh solid (Fig. 3a) and after sulfidation ($H_2S/H_2/CO_2$/He, 100 °C, 0.5 h) followed by regeneration (20% O_2/He, 750 °C, 10 h) (Fig. 3b). These photographs demonstrate a drastic change in the texture and morphology of the solid after sulfidation and regeneration. The large pore network in the fresh 5 Fe–15 Mn–40 Zn–40 Ti–O solid is evident, in agreement with its relatively high BET value (Table 1). The solid after sulfidation and regeneration consists of large aggregates of different sizes (2.5–9.0 μm; Fig. 2b). This result is in harmony with the drastic decrease in the BET area of the solid after sulfidation and regeneration (Table 1, Section 3.1.1). Novochinskii et al. [44] reported that in flat or flake crystal morphologies, the external mass transfer limitations during adsorption are much smaller than those encountered with cubes or prisms, supporting the view that sulfidation is dependent on particle morphology [45]. The texture of the 20 Fe–40 Zn–40 Ti–O solid was largely different than that of the 5 Fe–15 Mn–40 Zn–40 Ti–O solid. The former consisted of aggregates (large

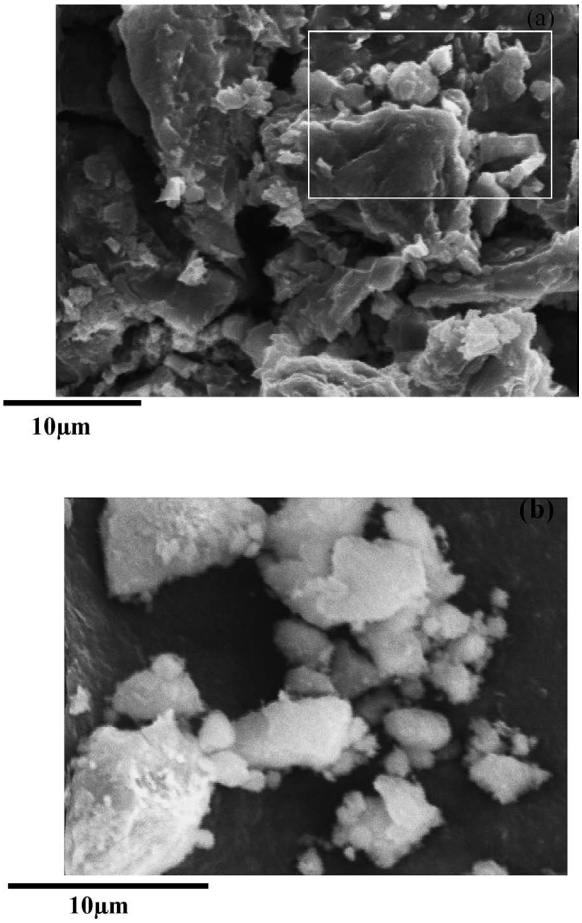

Fig. 3. SEM-photographs of the 5 Fe–15 Mn–40 Zn–40 Ti–O solid. (a) Fresh (calcined in 20% O_2/He, 500 °C, 4 h); (b) after sulfidation ($H_2S/H_2/CO_2$/He at 100 °C, 0.5 h) followed by regeneration (20% O_2/He, 750 °C, 10 h).

particles), in accordance with its low BET surface area (see Table 1). The aggregation of the particles is a result of grain fusion in the solid [46]. This suggestion is supported by the XPS results, which showed metal cation migration to inner and outer layers during sulfidation and regeneration (see Section 3.1.6).

3.1.4. H_2-TPR studies

Fig. 4a presents H_2-TPR traces obtained with the Fe–Mn–Zn–Ti–O series of solids. The 5 Fe–15 Mn–40 Zn–40 Ti–O solid shows a TPR trace characterized by a broad but symmetrical peak in the 275–800 °C range. As the amount of Fe in the solid increases, the H_2 TPR trace becomes broader and consists of a number of peaks. Thus, introducing more Fe ions (Fe^{2+}/Fe^{3+}) in the oxide lattice of Fe–Mn–Zn–Ti–O increases the amount of reducible oxygen species, reducing the strength of the M–O–M′ bonds. The maximum reduction rate (140 μmol/(g min)) observed for the 20 Fe–40 Zn–40 Ti–O solid is the lowest obtained in the oxides (185 μmol/(g min) for the 5 Fe–15 Mn–40 Zn–40 Ti–O and 210 μmol/(g min) for the remaining two solids). At 750 °C, the reduction rate of 5 Fe–15 Mn–40 Zn–40 Ti–O and 10 Fe–10 Mn–40 Zn–40 Ti–O solids approaches zero, whereas that of 15 Fe–5 Mn–40 Zn–40 Ti–O exhibits its highest value (210 μmol/(g min)). By integrating the H_2-TPR traces, the amount of H_2 consump-

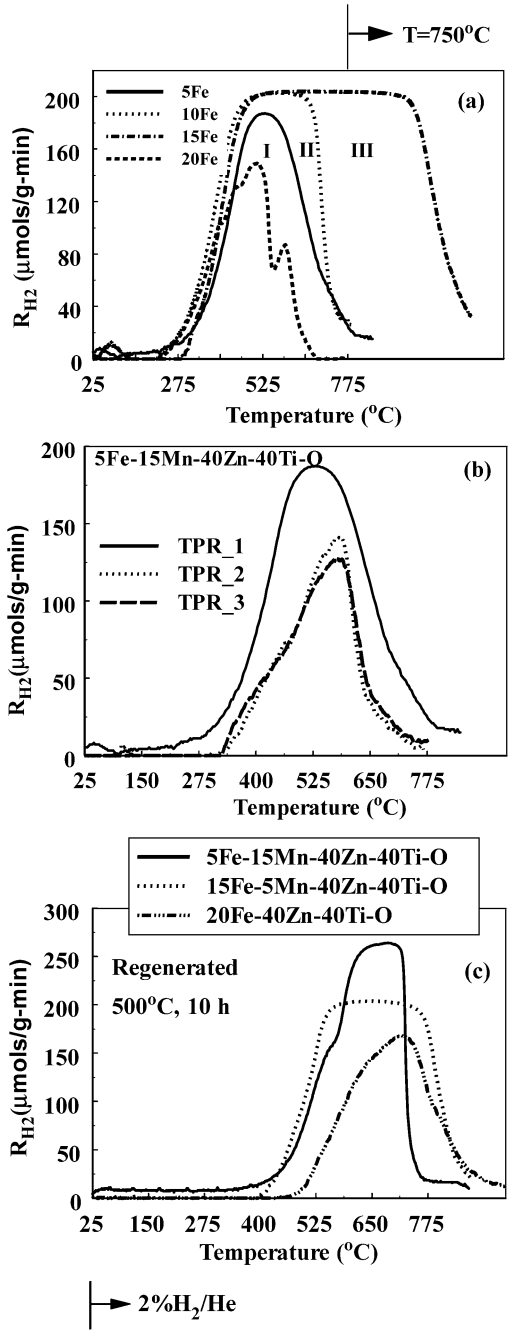

Fig. 4. (a) Hydrogen temperature-programmed reduction (H_2-TPR) profiles obtained over the fresh Fe–Mn–Zn–Ti–O series of solids. (b) H_2-TPR profiles obtained on 5 Fe–15 Mn–40 Zn–40 Ti–O solid during three consecutive oxidation/reduction cycles: 20% O_2/He (500 °C, 2 h) → 2% H_2/He (TPR), repeat cycle. (c) H_2-TPR profiles obtained over the regenerated 5 Fe–15 Mn–40 Zn–40 Ti–O, 15 Fe–5 Mn–40 Zn–40 Ti–O and 20 Fe–40 Zn–40 Ti–O solids. $F_{H_2/He} = 50$ NmL/min; $\beta = 30$ °C/min; $W = 0.2$ g. Regeneration conditions: 20% O_2/He, 500 °C, 10 h.

tion and equivalent reducible lattice oxygen can be estimated. This value was found to be 1794 μmol O/g for 5 Fe–15 Mn–40 Zn–40 Ti–O, 2307 μmol O/g for 10 Fe–10 Mn–40 Zn–40 Ti–O, 4469 μmol O/g for 15 Fe–5 Mn–40 Zn–40 Ti–O, and 1078 μmol O/g for 20 Fe–40 Zn–40 Ti–O solid.

In the 20 Fe–40 Zn–40 Ti–O solid, two not well-resolved reduction peaks appear (Fig. 4a). The first peak appears in the 200–525 °C range with a shoulder in the low-temperature range, while the second narrow one in the 525–670 °C range. These peaks reflect the reduction of oxygen species in the main crystalline phases of the solid ($ZnTiO_3$, $ZnFe_2O_4$, TiO_2, and Fe_2O_3; Table 2). According to our previous studies [28], a minor part of the low-temperature TPR peak was assigned to the reduction of $ZnTiO_3$, whereas the major part of it was attributed to the reduction of $ZnFe_2O_4$ [47,48]. In the presence of H_2, zinc ferrites decompose into ZnO and Fe_2O_3, and ferric oxide is further reduced to metallic iron [49]. The reduction profile of Fe_2O_3 has been reported to present two peaks, at 327 and 527 °C, corresponding to the reduction processes of $Fe_2O_3 \rightarrow Fe_3O_4$ and $Fe_3O_4 \rightarrow Fe$ [50], respectively; the high temperature peak reflects the reduction of Fe^{3+} to Fe^0. H_2-TPR studies conducted on TiO_2 single-metal oxide also prepared by the sol–gel method showed that the H_2-TPR trace consists of a symmetrical peak ($T_M = 660$ °C) with a maximum reduction rate of 30 μmol H_2/(g min). According to these results, a small contribution of TiO_2 reduction cannot be excluded from the TPR trace of 20 Fe–40 Zn–40 Ti–O solid (Fig. 4a).

The reduction profile of 5 Fe–15 Mn–40 Zn–40 Ti–O solid is related to the reduction of (Mn,Zn)MnO_3, $ZnFe_2O_4$, and $ZnTiO_3$ (the main crystalline phases according to XRD studies). The reduction process of $ZnMnO_3$ is a stepwise process [51]: $ZnMnO_3 \rightarrow ZnMnO_{2.5}$ (327 °C) → ZnO + Mn_2O_3 (527 °C) → MnO → Mn. The different size of the oxygen "pools" reduced, as reflected by the broadness of areas II and III, can be assigned to the different Fe/Mn ratios and the interaction of Fe and Mn cations, which regulate not only the percentage of each in the aforementioned crystal phases, but also the reduction mechanism of the oxides (shrinking core vs. nucleation model), as reflected by the different shapes of the TPR traces [51,52].

The redox behavior of the 5 Fe–15 Mn–40 Zn–40 Ti–O solid for three consecutive TPR runs is presented in Fig. 4b. After calcination in 20% O_2/He at 500 °C for 2 h, a H_2-TPR run was made; this is termed a redox cycle. A lower maximum reduction rate (140 μmol/(g min)) is obtained during the second redox cycle compared with the first cycle (190 μmol/(g min)). In contrast, the TPR trace of the third redox cycle is very similar to that of second redox cycle. The amount of hydrogen consumed is 1794 μmol H_2/g for the first redox cycle, 829 μmol H_2/g for the second cycle, and 850 μmol H_2/g for the third cycle. During the first and second redox cycles, structural changes occurred in the solid that influenced the strength of the M–O–M′ bonds in the various metal oxide lattices present. It appears that these structural changes become permanent after the second redox cycle.

Fig. 4c presents H_2-TPR traces obtained over the 5 Fe–15 Mn–40 Zn–40 Ti–O, 15 Fe–5 Mn–40 Zn–40 Ti–O, and 20 Fe–40 Zn–40 Ti–O solids after exposure to the $H_2S/H_2/CO_2$/He gas mixture at 100 °C for 0.5 h followed by regeneration at 500 °C for 10 h. The 15 Fe–5 Mn–40 Zn–40 Ti–O solid presents a broad reduction peak, in the 380–800 °C range, whereas the 5 Fe–15 Mn–40 Zn–40 Ti–O solid has a narrower peak, in the 400–750 °C range. The 20 Fe–40 Zn–40 Ti–O solid presents a reduction peak starting at a higher temperature (480 °C). The

amount of reducible lattice oxygen is 1914 μmol O/g for the 5 Fe–15 Mn–40 Zn–40 Ti–O solid, 2103 μmol O/g for the 15 Fe–5 Mn–40 Zn–40 Ti–O solid, and 1311 μmol O/g for the 20 Fe–40 Zn–40 Ti–O solid. Comparing the results of Figs. 4a and 4c shows that the amount of reducible oxygen increases by 6.7 and 22% after sulfidation and regeneration of the 5 Fe–15 Mn–40 Zn–40 Ti–O and 20 Fe–40 Zn–40 Ti–O solids, respectively. In contrast, a significant decrease (by 53%) in the amount of reducible oxygen is observed for the 15 Fe–5 Mn–40 Zn–40 Ti–O solid. Because the BET surface area of the 20 Fe–40 Zn–40 Ti–O solid is low and remains so after sulfidation and regeneration, the major part of the reducible oxygen corresponds to that in the bulk of the solid. But the 5 Fe–15 Mn–40 Zn–40 Ti–O solid preserves a major part of its surface area after sulfidation and regeneration, so the TPR trace reflects both the reduction of surface (low temperature range) and bulk (high temperature range) oxygen. According to the XPS results (Section 3.1.6), after regeneration at 500 °C, the 5 Fe–15 Mn–40 Zn–40 Ti–O and 20 Fe–40 Zn–40 Ti–O solids preserve 9.6 and 7.8 at% S on their surface, respectively (mainly as SO_4^{2}). The increase in reducible oxygen could also be due to sulfate reduction [53].

Comparing the nominal Fe/Mn ratios with those revealed by XPS studies for the 5 Fe–15 Mn–40 Zn–40 Ti–O and 15 Fe–5 Mn–40 Zn–40 Ti–O solids demonstrates that the former solid presents a surface enriched in Fe, whereas the latter solid has a surface enriched in Mn. The various Mn oxidation states facilitate lattice oxygen reduction, and thus a larger amount of reducible oxygen is expected, as indeed was obtained (TPR traces). Another important result from the TPR traces of Fig. 4 is that besides the fact that two or more phases are present in all of the Fe–Mn–Zn–Ti–O solids (see the XRD and Raman results), only one TPR peak is obtained, suggesting that reduction of the various crystalline phases occurs with essentially similar activation energy values [51,52]. Table 3 reports the amounts of lattice oxygen reduced in the 25–750 °C range (Fig. 4) as a function of Fe–Mn–Zn–Ti–O solid composition.

Table 3
Amounts of H_2 consumed or lattice oxygen reduced (μmol/g) during TPR experiments

Solid composition	Amount of lattice oxygen reduced (μmol/g)
5 Fe–15 Mn–40 Zn–40 Ti–O	1794[a]
	829[b]
	850[c]
	1914.2[d]
10 Fe–5 Mn–40 Zn–40 Ti–O	2307[a]
15 Fe–5 Mn–40 Zn–40 Ti–O	4469.9[a]
	1331[b]
	1359[c]
	2103[d]
20 Fe–40 Zn–40 Ti–O	1078.5[a]
	1311[d]

[a] Reduction was conducted after calcination at 500 °C for 2 h.
[b] 2nd TPR conducted after[a].
[c] 3rd TPR conducted after[b].
[d] TPR conducted after sulfidation ($H_2S/H_2/CO_2$/He) at 100 °C for 0.5 h followed by regeneration at 500 °C for 10 h.

3.1.5. Surface acidity and basicity studies—correlation with H_2S uptake

Table 4 reports comparative results of acidity measurements (NH_3-TPD) performed on the Fe–Mn–Zn–Ti–O series of solids as fresh (calcined at 500 °C for 4 h), after exposure to the adsorption mixture of $H_2S/H_2/CO_2$/He at 25 °C for 0.5 h, and after regeneration in 20% O_2/He at 500 °C for 4 h after sulfidation. In fresh solids, surface acidity decreases with increasing Fe/Mn molar ratio. This result agrees with the decreased Mn at% surface concentration found on XPS (see Section 3.1.6), where Mn^{4+} behaves as a stronger Lewis acid site. The same conclusion could be drawn by comparing the NH_3 uptakes of the fresh 5 Fe–15 Mn–40 Zn–40 Ti–O (525 μmol NH_3/g) and 5 Fe–5 Mn–45 Zn–45 Ti–O (338 μmol NH_3/g) solids, where the surface acidity is due mainly to the Mn-containing species ($ZnMnO_3$ and Mn–Zn ferrite) [51]. In the crystalline phase of $ZnMnO_3$, the presence of Zn^{2+} and Mn^{4+} cations with a different charge/radii (q/r) ratio leads to the formation of acid sites of varying strengths [51]. We can draw the same conclusion by comparing the surface acidity of 5 Fe–5 Mn–45 Zn–45 Ti–O and 7 Fe–3 Mn–45 Zn–45

Table 4
NH_3 and CO_2 uptakes measured during TPD experiments on Fe–Mn–Zn–Ti–O mixed metal oxides prepared by the sol–gel method

Solid composition	Uptake (μmol/g)					
	Fresh[a]		After sulfidation[b]		After regeneration[c]	
	NH_3	CO_2	NH_3	CO_2	NH_3	CO_2
5 Fe–15 Mn–40 Zn–40 Ti–O	525	5.0	160	5.0	73	4.0
10 Fe–10 Mn–40 Zn–40 Ti–O	249.4	21.2	–	–	–	–
15 Fe–5 Mn–40 Zn–40 Ti–O	145	11.8	279	4.0	213	4.0
20 Fe–40 Zn–40 Ti–O	112	6.0	166	4.0	156	4.0
5 Fe–5 Mn–45 Zn–45 Ti–O	338	17.9				
7 Fe–3 Mn–45 Zn–45 Ti–O	295	16.9				

[a] The solid was calcined in 20% O_2/He at 500 °C for 4 h.
[b] The solid was treated in 0.06% H_2S/25% H_2/7.5% CO_2/He gas mixture at 25 °C for 0.5 h.
[c] The solid was treated in 0.06% H_2S/25% H_2/7.5% CO_2/He gas mixture followed by regeneration with 20% O_2/He at 500 °C for 4 h.

Ti–O solids; decreasing the Mn mol% by 2 percentage units decreases the NH_3 uptake by 13%. For the 5 Fe–15 Mn–40 Zn–40 Ti–O, 10 Fe–10 Mn–40 Zn–40 Ti–O, and 15 Fe–5 Mn–40 Zn–40 Ti–O solids, the surface atomic concentration of Mn decreases (see Section 3.1.6), as does the surface acidity (Table 4).

After sulfidation, the surface acidity of the solids varies according to the Fe/Mn surface molar ratio. For example, the surface acidity drops significantly (by 70%) for the 5 Fe–15 Mn–40 Zn–40 Ti–O solid, whereas it increases by 92% for the 15 Fe–5 Mn–40 Zn–40 Ti–O solid and by 48% for the 20 Fe–40 Zn–40 Ti–O solid. After sulfidation followed by regeneration, the surface acidity of 5 Fe–15 Mn–40 Zn–40 Ti–O, 15 Fe–5 Mn–40 Zn–40 Ti–O, and 20 Fe–40 Zn–40 Ti–O solids is reduced based on the Fe/Mn molar ratio (Table 4). The reduced acidity of the regenerated 5 Fe–15 Mn–40 Zn–40 Ti–O solid can be explained as follows. The Fe/Mn surface molar ratio is practically the same in both the fresh and the sulfided states of the solid (0.40 vs. 0.38; see Section 3.1.6). After regeneration, the surface acidity drops significantly, possibly due to extensive surface reconstruction. The latter is identified by the increased S at% surface composition measured after regeneration, a kinetically limited process that leads to S migration from the bulk to the surface. On the other hand, the surface basicity of the 5 Fe–15 Mn–40 Zn–40 Ti–O solid remains practically constant after sulfidation and decreases by 20% only after regeneration (Table 4).

Based on the results of Table 4, the surface acid character of the sol–gel-prepared mixed-metal oxides (fresh) is predominant compared with their surface basic character. These results can be explained based on the findings of Ziolek et al. [54], who contended that three possible H_2S adsorption steps can be considered. The first of these steps is exchange of the oxygen of metal oxide for sulfur, dissociation of H_2S into HS^- and H^+ (the latter found as –OH species) and a coordinatively bonded H_2S. Travert et al. [55] studied the adsorption of H_2S on SiO_2, Al_2O_3, TiO_2, and ZrO_2 by infrared (IR) spectroscopy using CO as a probe molecule. They reported that the decrease in Lewis acidity was due to the occupation of acidic sites by both the adsorbed H_2S and the intermediate products of its dissociation. An increased number of Brönsted acid sites, as well as modification of their strength, was also observed. As discussed earlier, the fresh solid with 20 mol% Fe exhibits the lowest concentration of acid sites after sulfidation and the lowest H_2S uptake (see Section 3.2), but demonstrates the strongest M–O–M′ bonds (see Section 3.1.4). These results can be explained by considering that the pathways of oxygen exchange for sulfur and/or H_2S dissociation are not the main paths for the sulfidation mechanism over the 20 Fe–40 Zn–40 Ti–O solid. It is suggested that a dissociative coordination of H_2S on Lewis acid sites is favored instead. The products of H_2S adsorption lead to increased Brönsted acidity. The acidity of the 20 Fe–40 Zn–40 Ti–O solid after sulfidation is 1.5 times higher than that of the fresh sample. In contrast, an associative coordination of H_2S on Lewis acid sites is favored over the 5 Fe–15 Mn–40 Zn–40 Ti–O solid.

3.1.6. X-Ray photoelectron spectroscopy studies

Table 5 reports the surface metal and sulfur at% composition of the Fe–Mn–Zn–Ti–O H_2S solid adsorbents after exposure to different gas atmospheres. The 5 Fe–15 Mn–40 Zn–40 Ti–O solid shows decreases in Fe, Mn, and Zn surface composition by 17, 13, and 7%, respectively, and a minor increase in Ti surface composition after exposure of the solid to the $H_2S/H_2/CO_2$/He gas mixture. The Fe/(Fe + Mn + Zn + Ti) ratio appears to be lower than in the case of the fresh solid (6.5 vs. 7.5%), whereas after regeneration (500 °C, 4 h), it appears to be practically the same in both the fresh and the regenerated solids. In contrast, after regeneration at 750 °C for 10 h, the Fe/(Fe + Mn + Zn + Ti) ratio appears to be higher than that of the fresh solid (8.5%

Table 5
Surface at% composition of the Fe–Mn–Zn–Ti–O series of solids (fresh, sulfated and regenerated) derived from XPS analyses

Solid composition	Atom% surface composition				
	Ti	Zn	Fe	Mn	S
5 Fe–5 Mn–45 Zn–45 Ti–O	52.3[a]	38.2	4.2	5.3	–
7 Fe–3 Mn–45 Zn–45 Ti–O	45.2[a]	41.1	9.5	4.2	–
5 Fe–15 Mn–40 Zn–40 Ti–O	39.4[a]	34.5	7.5	18.6	–
	40.9[b]	31.9	6.2	16.2	4.8
	41.7[c]	28.2	8.1	17.0	5.0
	29.7[d]	38.0	6.5	16.2	9.6
10 Fe–10 Mn–40 Zn–40 Ti–O	45.1[a]	35.4	8.6	10.9	–
15 Fe–5 Mn–40 Zn–40 Ti–O	38.7[a]	44.0	10.4	6.9	–
	31.8[d]	45.5	9.1	6.6	7.0
20 Fe–40 Zn–40 Ti–O	37.68[a]	45.79	16.51	–	–
	35.2[b]	41.8	15.1	–	7.9
	33.43[c]	46.49	20.07	–	–
	31.3[d]	48.3	12.6	–	7.8

[a] After synthesis, the solid was calcined in 20% O_2/He at 500 °C for 4 h.
[b] The solid was treated in 0.06% H_2S/25% H_2/7.5% CO_2/He at 100 °C for 0.5 h.
[c] After treatment in 0.06% H_2S/25% H_2/7.5% CO_2/He, the solid was regenerated in 20% O_2/He at 750 °C for 10 h.
[d] After treatment in 0.06% H_2S/25% H_2/7.5% CO_2/He, the solid was regenerated in 20% O_2/He at 500 °C for 4 h.

vs. 7.5%). Based on these results, it appears that treatment of the fresh 5 Fe–15 Mn–40 Zn–40 Ti–O solid with the given H_2S-containing gas mixture causes migration of Fe to the inner layers of the solid. Regeneration of the solid at 500 °C is sufficient to recover the Fe surface concentration, whereas regeneration at 750 °C results in a surface enriched with Fe. The lower surface atomic concentration of Zn after regeneration at 750 °C for 10 h is consistent with Zn migration to the inner layers of the solid. This migration is in harmony with a grain–grain fusion in solid particles [46], as evidenced by the present SEM studies.

We note the following points about the 20 Fe–40 Zn–40 Ti–O solid, which exhibits the lowest H_2S uptakes (see Section 3.2.1):

(a) After the solid was exposed to the $H_2S/H_2/CO_2$/He gas mixture, 8.5, 8.7, and 6.6% decreases in Fe, Zn, and Ti surface concentrations, respectively, occurred (Table 5).
(b) The Fe/(Fe + Zn + Ti) ratio appears to be higher after sulfidation compared with the fresh sample.
(c) After regeneration at 500 °C, the Fe/(Fe + Zn + Ti) ratio further decreased, whereas after regeneration at 750 °C, it was higher than that of the fresh solid (Fe surface enrichment).

XPS results show that the 5 Fe–15 Mn–40 Zn–40 Ti–O solid is more susceptible to Fe migration through inner layers (i.e., during sulfidation) or outer layers (i.e., during regeneration) than the 20 Fe–40 Zn–40 Ti–O solid. These results are in good agreement with the findings of BET and SEM studies (Sections 3.1.1 and 3.1.3) demonstrating that the 20 Fe–40 Zn–40 Ti–O fresh solid consists of aggregates and has a significantly lower BET area (1.4 m^2/g) than the 5 Fe–15 Mn–40 Zn–40 Ti–O solid (107.4 m^2/g). It is obvious that the metal cation diffusion mechanism that has been suggested for the propagation of sulfidation at low temperatures (<100 °C) is facilitated in a solid with high surface area [5,45].

After sulfidation, the S surface atomic concentration is 4.8% in the 5 Fe–15 Mn–40 Zn–40 Ti–O solid and 7.9% in the 20 Fe–40 Zn–40 Ti–O solid (Table 5). The presence of sulfur and sulfates after sulfidation and regeneration is in agreement with reports in the literature [56]. Because the escape depth of the photoelectrons in the solid analyzed by XPS is confined to 3–5 nm, only the topmost layers of the solid particles are concerned. Part of S has penetrated in the inner layers of the 5 Fe–15 Mn–40 Zn–40 Ti–O solid, a procedure that is more difficult in the 20 Fe–40 Zn–40 Ti–O solid as discussed earlier.

Fig. 5 presents XPS spectra of S 2p core electron levels obtained in the 5 Fe–15 Mn–40 Zn–40 Ti–O solid after sulfidation followed by regeneration at 750 °C for 10 h (R-1 spectrum) and 500 °C for 4 h (R-2 spectrum). After sulfidation followed by regeneration at 500 °C, XPS spectra corresponding to 15 Fe–5 Mn–40 Zn–40 Ti–O (R-3) and 20 Fe–40 Zn–40 Ti–O (R-4) solids were obtained. The S 2p XP peak at 168 eV corresponds to S–O moieties and is attributed to SO_4^{2-} [57]. The S 2p XP peak at 162 eV corresponds to S^{2-} in the case of sulfided samples. All fresh samples present Mn $2p_{3/2}$ BEs (642.3–642.5 eV), which correspond to Mn^{4+} [58], result which is in harmony with the presence of the $ZnMnO_3$ phase (see XRD studies). The Fe $2p_{3/2}$ peak with a binding energy at 711–712 eV corresponds to an Fe(III)-O environment according to Thomas et al. [59]. The 5 Fe–15 Mn–40 Zn–40 Ti–O solid after sulfidation presents Mn $2p_{3/2}$ BEs equal to 641.6 eV, which accounts for Mn^{3+} [58] (Mn is reduced after sulfidation). The following reactions are consistent with the XPS data:

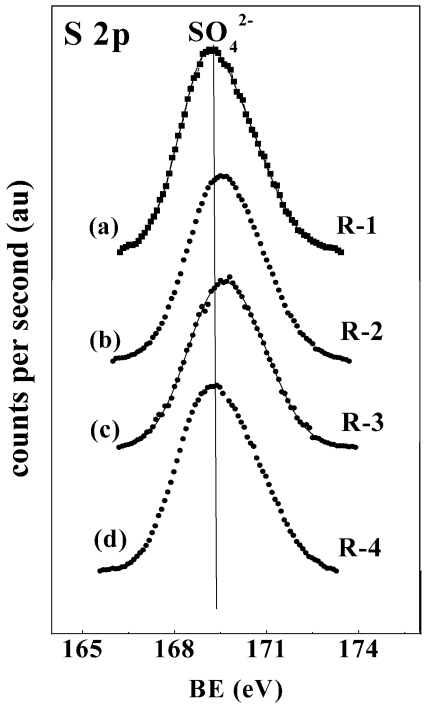

Fig. 5. X-Ray photoelectron spectra of S 2p core electron level obtained on the 5 Fe–15 Mn–40 Zn–40 Ti–O solid (a) after sulfidation and regeneration (750 °C, 10 h) (R-1); (b) after sulfidation and regeneration (500 °C, 4 h) (R-2); (c) after sulfidation and regeneration at 500 °C for 4 h of 15 Fe–5 Mn–40 Zn–40 Ti–O (R-3) and (d) 20 Fe–40 Zn–40 Ti–O (R-4) solids.

$$ZnMnO_3 \rightarrow ZnO + Mn^{IV}O_2 \quad \text{(dissociation by } H_2S\text{)} \qquad (1)$$

and

$$2MnO_2 + 4H_2S \rightarrow Mn_2^{(III)}S_3 + 4H_2O + S \quad \text{(reduction by } H_2S\text{)}. \qquad (2)$$

After regeneration, Mn species are reoxidized to tetravalent Mn ions. In contrast, sulfidation hardly influences the electronic state of iron, because the same binding energy of Fe $2p_{3/2}$ for the fresh and sulfided samples was obtained. The oxidation states of Zn^{2+} and Ti^{4+} appeared unaffected by the applied sulfidation and regeneration conditions.

3.1.7. Mössbauer studies

Table 6 reports Mössbauer data extracted from the spectra recorded at 25 °C on the fresh, sulfided (100 °C, 0.5 h), and regenerated (500 °C/4 h or 750 °C/10 h) 5 Fe–15 Mn–40 Zn–40 Ti–O and 20 Fe–40 Zn–40 Ti–O solids. For the fresh 5 Fe–15 Mn–40 Zn–40 Ti–O solid, the isomer shift (IS) (δ_{Fe}) equals 0.33 mm/s. This value is typical of Fe^{3+} located in the B-sites of Mn–Zn ferrite nanoparticles [60]. Given that pure

Table 6
Mössbauer parameters corresponding to the 5 Fe–15 Mn–40 Zn–40 Ti–O and 20 Fe–40 Zn–40 Ti–O solids as fresh, after sulfidation and regeneration

Solid composition	δ_{Fe} (mm/s)	ΔE_q (mm/s)	$\Gamma/2$ (mm/s)
5 Fe–15 Mn–40 Zn–40 Ti–O	0.33[a]	0.53	0.19
	0.34[b]	0.57	0.19
	0.34[c]	0.47	0.17
	0.34[d]	0.57	0.21
20 Fe–40 Zn–40 Ti–O	0.37[a]	0.43	0.17
	0.37[b]	0.45	0.17
	0.37[c]	0.44	0.17
	0.37[d]	0.45	0.17

[a] The solid was calcined in 20% O_2/He at 500 °C for 4 h.
[b] The solid was treated in 0.06% H_2S/25% H_2/7.5% CO_2/He at 100 °C for 0.5 h.
[c] The solid was treated in 0.06% H_2S/25% H_2/7.5% CO_2/He followed by regeneration in 20% O_2/He at 750 °C for 10 h.
[d] The solid was treated in 0.06% H_2S/25% H_2/7.5% CO_2/He followed by regeneration in 20% O_2/He at 500 °C for 4 h.

$ZnFe_2O_4$ spinel phase has $\Delta E_q = 0.36$ mm/s at room temperature, $MnFe_2O_4$ is magnetic at room temperature, and that a relatively low calcination temperature (500 °C) was used, the presence of a Mn–Zn ferrite crystal phase ($(Mn,Zn)Fe_2O_4$) is suggested. After exposure of the 5 Fe–15 Mn–40 Zn–40 Ti–O solid to the $H_2S/H_2/CO_2$/He gas mixture, the IS parameter is preserved within experimental accuracy (0.34 mm/s). This result strongly supports the view that the Fe^{3+} environment hardly has been influenced by the given sulfidation process. This is in agreement with the XPS results (see Section 3.1.6). After sulfidation, the IS and ΔE_q values suggest the presence of FeS_2 [61]. The regeneration seems to have drastically influenced the structural properties of the 5 Fe–15 Mn–40 Zn–40 Ti–O solid. After regeneration at 500 °C, the IS and ΔE_q values of the solid remain the same as in the case after sulfidation. But after regeneration at 750 °C, the ΔE_q value changes to 0.57 mm/s. The values obtained for the Mössbauer parameters are attributed to the presence of FeS_2 (marcasite). The same value of isomer shift observed in the fresh sample after exposure to the H_2S-containing gas mixture and that after regeneration signifies the same electron density for the Fe nucleus.

In the 20 Fe–40 Zn–40 Ti–O solid, the IS and ΔE_q parameters are similar for the fresh, sulfided, and regenerated solids (Table 6) within the limits of experimental error. The same value of IS and quadrapole splitting (0.43–0.45 mm/s) observed corresponds to the same electron density and environment geometry for the Fe nucleus. Thus the Mössbauer results obtained suggest that 5 Fe–15 Mn–40 Zn–40 Ti–O solid is more susceptible than the 20 Fe–40 Zn–40 Ti–O solid to electronic perturbations and structural distortions during sulfidation. This finding is in harmony with the XRD (Section 3.1.2), XPS (Section 3.1.6), and Raman (Section 3.1.8) studies.

Comparing the solid phase composition in 5 Fe–15 Mn–40 Zn–40 Ti–O and 20 Fe–40 Zn–40 Ti–O solids, it can be stated that Mn plays a key role in defining the cation distribution in the A and B sites in the present spinel phases ($Fe^{3+} + Mn^{2+} \Leftrightarrow Fe^{2+} + Mn^{3+}$). In turn, this regulates the adsorption of H_2S, in which 5 Fe–15 Mn–40 Zn–40 Ti–O exhibits significantly larger H_2S uptake than the 20 Fe–40 Zn–40 Ti–O solid (see Section 3.2).

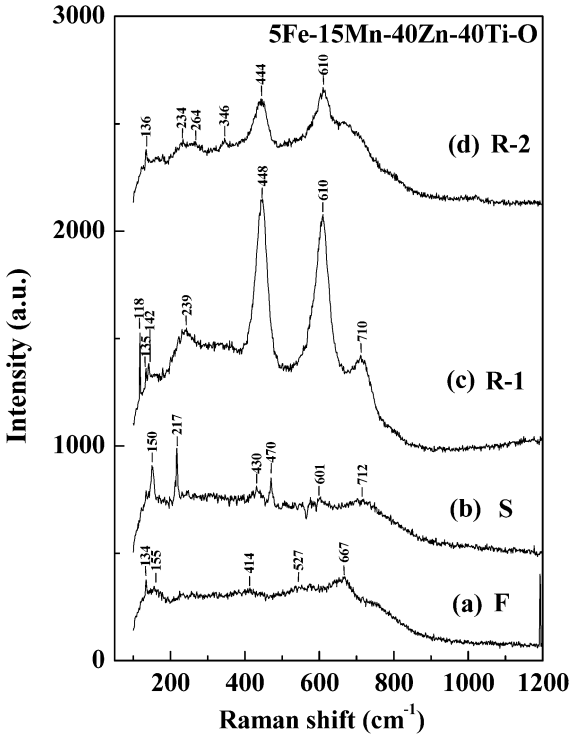

Fig. 6. Raman spectra of 5 Fe–15 Mn–40 Zn–40 Ti–O solid. (a) Fresh, F (calcined in 20% O_2/He, 500 °C, 4 h); (b) after sulfidation, S ($H_2S/H_2/CO_2$/He, 100 °C, 0.5 h); (c) after sulfidation followed by regeneration, R-1 (20% O_2/He, 750 °C, 10 h); (d) after sulfidation followed by regeneration, R-2 (20% O_2/He, 500 °C, 4 h).

3.1.8. Raman studies

Fig. 6a presents the Raman spectrum obtained on the fresh 5 Fe–15 Mn–40 Zn–40 Ti–O solid. The peaks at 527 and 676 cm^{-1} are assigned to $(Mn,Zn)Fe_2O_4$ [62,63], in harmony with the XRD and Mössbauer studies (see Tables 2 and 6). The broadness of the peak is consistent with the crystallinity of ferrite (see also Fig. 1). Fig. 6b presents the Raman spectrum obtained on the 5 Fe–15 Mn–40 Zn–40 Ti–O solid after exposure to the $H_2S/H_2/CO_2$/He gas mixture at 100 °C for 0.5 h. The broad peak at 712 cm^{-1} is assigned to the presence of nonstoichiometric ferrite $(Mn_xZn_{1-x})Fe_2O_4$ ($x < 1$) [62,63]. The shift of this band compared with the peak wavenumber is due to the distorted Mn–Zn ferrite phase [62–64]. The bands at 150, 217, and 470 cm^{-1} are typical of sulfur [65]. The band at 470 cm^{-1} is somewhat broader than the sulfur typical Raman band, very likely because of the presence of polysulfides [66,67].

Figs. 6c and 6d present Raman spectra obtained on the 5 Fe–15 Mn–40 Zn–40 Ti–O solid after its regeneration at 750 and 500 °C, respectively. According to the literature [68], the broad bands centered at 237, 448, and 610 cm^{-1} are typical of disordered manganites, almost independently of the averaged crystallographic long-range symmetry (orthorhombic [69] or rhombohedral [70]), the degree of doping [71], or the nature of the

element at the A site. Thus these bands reflect some very basic structural features. The line near 230 cm^{-1} was assigned to a rotational-like distortion of MnO_6 octahedra due to the mismatch between the average ionic radius (r_a) of the A site species and the ionic radius (r_{Mn}) of Mn [72,73]. The other two bands near 450 and 610 cm^{-1} are related to the Jahn–Teller octahedral distortions.

By increasing the regeneration T from 500 to 750 °C, the three broad bands of $ZnMnO_3$ appear to be slightly shifted. After regeneration at 500 °C (Fig. 6d), the active Raman modes of $ZnMnO_3$ appear at 234, 444, and 610 cm^{-1}, whereas after regeneration at 750 °C, the band at 234 shifts to 239 cm^{-1} and the band at 444 shifts to 448 cm^{-1} (Fig. 6c). However, the difference in the Raman shift between the spectra shown in Figs. 6c and 6d is small and considered within the limits of experimental error (4 cm^{-1}). The absence of detection of $ZnMnO_3$ crystalline phase in the fresh sample is likely because this phase is ill-crystallized, whereas the opposite is true in the regenerated solid. In the case of regeneration at 500 °C, the successive calcination cycles led to better crystallization of $ZnMnO_3$; thus Raman bands appear more intense. In the case of regeneration at 750 °C, the $ZnMnO_3$ crystallites are much better formed, and the Raman bands appear even more intense.

After regeneration at 500 °C (Fig. 6d), a small peak (at 346 cm^{-1}) appears that can be assigned to the remaining sulfur ($S_2O_7^{2-}$) in the sample [74]. Such sulfur oxy-anion species were reported to be important intermediate species under the Claus reaction conditions on alumina-based catalysts [75]. These species are then reduced by H_2S to form S_x sulfur species. This is an important point, because it may suggest that oxygen is required to create oxidizing sites on the present metal oxides given the fact that after sulfidation (use of H_2S in the absence of oxygen) only polysulfide species were found, as previously discussed.

The S peaks at 150, 217, and 470 disappear (Fig. 6d). These results demonstrate that regeneration at 500 °C is capable of removing a fraction of sulfur from the sample. The peak at 710 cm^{-1} corresponds to $(Mn_xZn_{1-x})Fe_2O_4$ [64], as also evidenced by the Mössbauer studies. Raman spectra obtained on the 20 Fe–40 Zn–40 Ti–O fresh solid (not presented here) confirmed the presence of Fe_2O_3 (222, 253, 303, 398 cm^{-1}), $ZnFe_2O_4$ (352, 521, 734 cm^{-1}), and TiO_2 (156, 438, 601 cm^{-1}) phases. After sulfidation and regeneration, practically the same peaks as those appearing in the fresh solid were obtained. The absence of the three typical peaks of sulfur demonstrates that sulfidation of this solid was limited to the surface. The opposite is true in the 5 Fe–15 Mn–40 Zn–40 Ti–O solid.

3.2. Transient H_2S uptake experiments

The H_2S uptake of the solids until saturation is obtained was studied by transient adsorption [28] from the $H_2S/H_2/CO_2/He$ gas mixture in the 25–100 °C range. The catalyst was pretreated in 20% O_2/He at 500 °C for 2 h, purged in He at 500 °C, and then cooled in He flow to the desired adsorption temperature. The H_2S uptakes were calculated according to the procedures described elsewhere [28].

3.2.1. Effect of Fe content and regeneration temperature

Fig. 7a presents results of H_2S uptake at 25 °C as a function of Fe content for the Fe–Mn–Zn–Ti–O series of solids as fresh and after exposure to the given H_2S-containing gas mixture followed by regeneration at 500 °C or 750 °C. Among the fresh samples, 5 Fe–15 Mn–40 Zn–40 Ti–O with the highest BET area (107.4 m^2/g) presents the highest H_2S uptake (2.4 mmol/g), whereas the 20 Fe–40 Zn–40 Ti–O solid with the lowest BET area (1.5 m^2/g) presents the lowest uptake (0.5 mmol/g). Based on these results, sulfidation of 20 Fe–40 Zn–40 Ti–O solid is limited to its outer layers, whereas sulfidation of 5 Fe–15 Mn–40 Zn–40 Ti–O is limited to its inner layers. These results are in harmony with the Raman results in which sulfidation of the 5 Fe–15 Mn–40 Zn–40 Ti–O solid showed the characteristic triplet of sulfur (150, 217, and 470 cm^{-1}) not observed in the case of sulfided 20 Fe–40 Zn–40 Ti–O solid. Kobayashi et al. [16,17] reported an H_2S uptake of 2.48 mmol/g on the fresh zinc ferrite powder sample at 450 °C from a gas stream of 1 vol% H_2S/N_2.

As shown in Fig. 7a, the Fe–Mn–Zn–Ti–O solids lose their H_2S uptake capacity to varying extents after regeneration at 500 °C for 4 h. There is an approximate 18% reduction in H_2S uptake for both 5 Fe–15 Mn–40 Zn–40 Ti–O and 20 Fe–40 Zn–40 Ti–O solids. Note that the 5 Fe–15 Mn–40 Zn–40 Ti–O solid exhibits a 5-fold greater H_2S uptake than the 20 Fe–40 Zn–40 Ti–O solid after regeneration at 500 °C. As clearly shown by XRD, Mössbauer, and Raman studies, the former solid is more prone to structural changes (increased crystallinity) than the latter during regeneration.

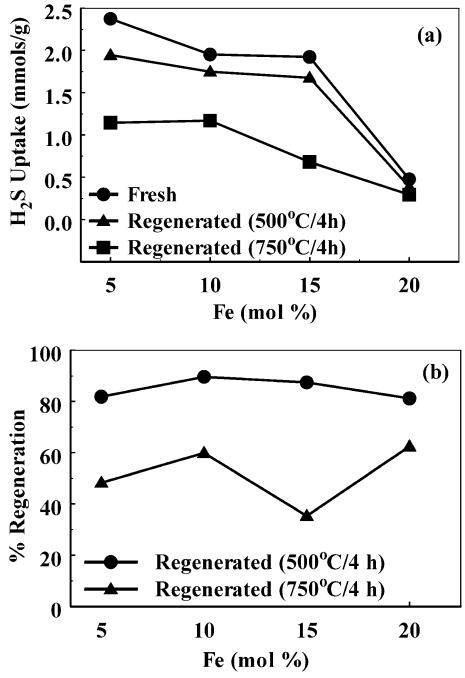

Fig. 7. (a) H_2S uptake (mmol/g) as a function of Fe content (mol%) in the Fe–Mn–Zn–Ti–O solids and regeneration conditions. (b) Regeneration percentage of Fe–Mn–Zn–Ti–O solids as a function of Fe content and regeneration conditions. Adsorption gas mixture: 0.06% H_2S/25% H_2/7.5% CO_2/He; $F = 30$ NmL/min; $W = 5$ mg.

After regeneration at 750 °C for 4 h, all Fe–Mn–Zn–Ti–O solids present lower H_2S uptakes. For example, decreases in H_2S uptake by 18 and 52% on the 5 Fe–15 Mn–40 Zn–40 Ti–O solid were obtained after regeneration at 500 and 750 °C, respectively. Given the fact that there is a nonlinear relationship between BET surface area and H_2S uptake, the large decrease of H_2S uptake after regeneration at 750 °C is partly attributed to the loss of BET area of the solids and their increased crystallite size. It is important to note that for the Fe–Mn–Zn–Ti–O solids the active sites for H_2S adsorption (sulfidation sites) are mostly Fe, Mn, and Zn metal cations, whereas Ti metal cations act as structural components favoring the formation of spinel phases and other mixed-metal oxide structures [76]. Another reason for the large decrease of H_2S uptake after regeneration at 750 °C is the loss of Zn as observed by XPS studies (see Table 3). Zinc is one of the active sites for initiating the sulfidation process.

The lower H_2S uptake exhibited by the solids after regeneration is also partly due to the presence of remaining sulfides (S^{2-}) and sulfates (SO_4^{2-}) in the bulk of the solid, the formation of which is favored in the presence of Mn [77]. Calcination in air of manganese sulfates at high temperatures (>750 °C) led to increased formation of manganese oxide [77]. Also note that the Fe-based H_2S adsorbents required the lowest regeneration temperature in air among other H_2S adsorbents without sulfate formation at the end [77].

The percentage regeneration of the solids as a function of Fe content is presented in Fig. 7b. The highest percentages of H_2S uptake recovery are obtained after regeneration of the solid at 500 °C, whereas the lowest percentage (30%) is obtained over the 15 Fe–5 Mn–40 Zn–40 Ti–O solid after regeneration at 750 °C for 4 h. The highest percentage of H_2S uptake recovery (81.9%) is obtained over the 5 Fe–15 Mn–40 Zn–40 Ti–O solid. This result is in harmony with the fact that this solid preserves its BET area after regeneration at 500 °C. After regeneration at 750 °C, the percentage recovery of H_2S uptake for the 5 Fe–15 Mn–40 Zn–40 Ti–O solid is reduced to 48.3%. The loss of BET area (see Table 1) and structural changes (see the Raman and Mössbauer results) are considered the main causes for the decreased percentage regeneration of the solid at 750 °C compared with 500 °C.

For the 5 Fe–15 Mn–40 Zn–40 Ti–O solid, H_2S uptake measurements at 25 °C were conducted from 0.06% H_2S/He and 0.06% H_2S/25% H_2/He gas mixtures. For the former gas composition, the H_2S uptake was found to be 3.8 mmol/g, whereas for the latter, the uptake was 1.34 mmol/g. Comparing these results with those from the 0.06% H_2S/25% H_2/7.5% CO_2/He gas mixture (2.4 mmol/g) leads to an intial conclusion that a competitive adsorption/interaction of H_2S, H_2, and CO_2 occurs on the given solid. Changes in the chemical environment of sulfidation sites due to the presence of CO_2 and H_2 cannot be excluded. In particular, the adsorption of CO_2 onto O^{n-} sites can cause changes in the acid character of surface sites responsible for H_2S chemisorption and accommodation of its derived HS^-, S^{2-}, and H^+ species.

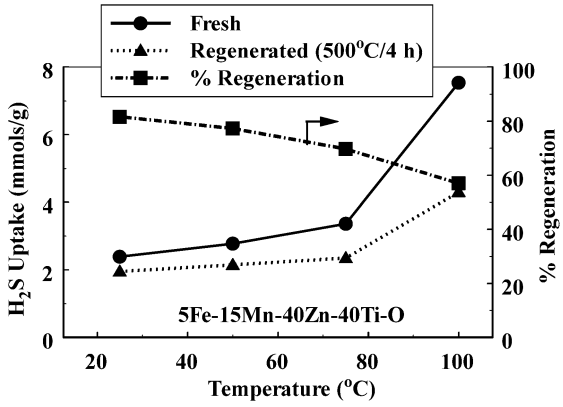

Fig. 8. (a) H_2S uptake (mmol/g) and percentage regeneration of 5 Fe–15 Mn–40 Zn–40 Ti–O solids as a function of adsorption temperature in the 25–100 °C range. Results are shown for the fresh solid and after its sulfidation followed by regeneration at 500 °C for 4 h.

3.2.2. *Effects of adsorption T*

Fig. 8 presents results of H_2S uptake as a function of adsorption temperature in the 25–100 °C range over the 5 Fe–15 Mn–40 Zn–40 Ti–O solid. For the fresh sample, there is an increase of H_2S uptake in the 25–100 °C range. In particular, there is an increase by a factor of 1.4 at 75 °C and by a factor of 3.2 at 100 °C compared with the uptakes obtained at 25 °C. A similar behavior is obtained on the regenerated solid at 500 °C. There is an increase in H_2S uptake in the whole temperature range of 25–100 °C. But the H_2S uptake of the regenerated solid at each individual temperature appears to decrease with respect to that obtained on the fresh sample. This behavior is due partly to the presence of remaining sulfur, and also to the loss of BET area after regeneration (Table 1). The formation of ZnS and FeS_2 was probed by XRD and Mössbauer studies, respectively, as discussed earlier. The percentage regeneration of the solid as a function of adsorption temperature is also presented in Fig. 8. The lowest percentage regeneration is obtained at 100 °C. This is likely due to the fact that at this temperature, sulfidation proceeded to a larger extent into the bulk of the solid, and as a result, the regeneration conditions applied were not so efficient.

3.2.3. *Correlation of H_2S uptake with BET*

According to previous reports [77], a key parameter in achieving acceptable H_2S uptakes at temperatures below 100 °C is the specific surface area of the solid. This provides immediate availability of sites for adsorption (first step of the sulfidation process). Fig. 9 shows BET area and H_2S uptake as a function of Fe content in the Fe–Mn–Zn–Ti–O solids. The decrease in BET area with increasing Fe content is accompanied by a decrease in H_2S uptake. The same type of BET area–H_2S uptake relationship has been observed over Zn–Ti–O and Mn–Zn–Ti–O solids [28]. These results strongly support the view that the interaction of H_2S with these solids is not confined to the surface. A solid-state diffusion of HS^- and S^{2-} species toward the bulk of the solid particles to eventually form metal sulfide compounds has been proposed [5]. The initial step of H_2S adsorption and the subsequent dissociation of the latter into HS^- and H^+ is followed by diffusion of HS^- and S^{2-} into the ox-

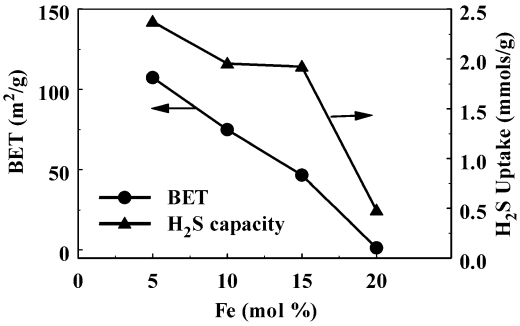

Fig. 9. Specific surface area (BET, m^2/g) and H_2S uptake (mmol/g) as a function of Fe content (mol%) in the fresh Fe–Mn–Zn–Ti–O series of solids. Adsorption conditions: 0.06% H_2S/25% H_2/7.5% CO_2/He, 25 °C; F = 30 NmL/min. Regeneration conditions: 20% O_2/He, 500 °C, 4 h.

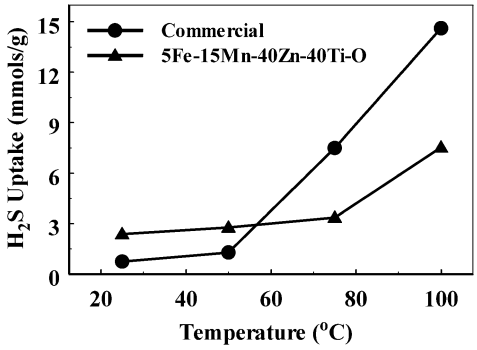

Fig. 10. H_2S uptake (mmol/g) as a function of adsorption temperature in the 25–100 °C range obtained on the 5 Fe–15 Mn–40 Zn–40 Ti–O and Ni-based commercial solid adsorbents. Adsorption gas mixture used: 0.06% H_2S/25% H_2/7.5% CO_2/He; F = 30 NmL/min.

ide lattice. Migration of the lattice oxygen to the surface of the solid also proceeds to form H_2O. However, bulk diffusion of anions is unlikely to occur at low temperatures, and thus surface reconstruction was proposed instead [5]. This mechanism is expected to depend on BET area and the details of solid crystals morphology [28].

3.2.4. Comparison of H_2S uptake of the sol–gel-prepared solids with a commercial Ni-based solid adsorbent

Fig. 10 compares the H_2S uptake obtained on the 5 Fe–15 Mn–40 Zn–40 Ti–O and commercial Ni-based H_2S solid adsorbents as a function of adsorption temperature. For the temperature range of 25–50 °C, the sol–gel-prepared solid has a greater H_2S uptake than the commercial one (2.4 vs. 0.75 mmol/g at 25 °C and 2.8 vs. 1.3 mmol/g at 50 °C). However, at 75 °C and 100 °C, the commercial adsorbent has a greater H_2S uptake (by a factor of 2.2 and 1.5, respectively). It appears that sulfidation of NiO to form NiS is facilitated at temperatures above 50 °C compared with $ZnMnO_3$, $(Mn,Zn)Fe_2O_4$, and $ZnTiO_3$ present in the 5 Fe–15 Mn–40 Zn–40 Ti–O solid. It is important to note that the commercial Ni–NiO/SiO_2 catalyst is not regenerable, as opposed to the presently developed 5 Fe–15 Mn–40 Zn–40 Ti–O solid adsorbent. Also note that 5 Fe–15 Mn–40 Zn–40 Ti–O appears to be the best solid synthesized in our laboratory so far for low-temperature H_2S adsorption for the given H_2S-containing gas mixture studied [28].

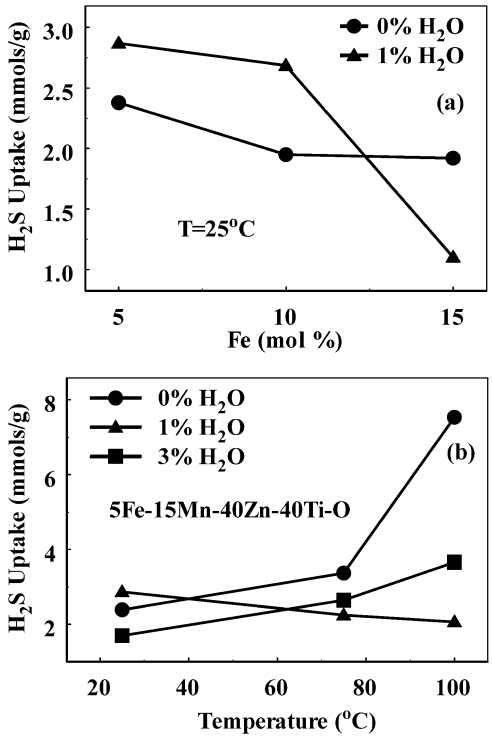

Fig. 11. (a) Effect of 1 vol% H_2O present in the adsorption gas mixture on the H_2S uptake (mmol/g) for the x mol% Fe–Mn–Zn–Ti–O series of solids. (b) Effect of H_2O concentration and temperature on the H_2S uptake (mmol/g) for the 5 Fe–15 Mn–40 Zn–40 Ti–O solid in the 25–100 °C range. Adsorption conditions: 0.06% H_2S/25% H_2/7.5% CO_2/x% H_2O/He, x = 1, 3 vol%; F = 30 NmL/min.

3.2.5. Effect of H_2O on the H_2S uptake

3.2.5.1. 5 Fe–15 Mn–40 Zn–40 Ti–O solid Fig. 11a presents the effect of 1 vol% H_2O present in the adsorption gas mixture on the H_2S uptake at 25 °C on the fresh x% Fe–Mn–Zn–Ti–O solids as a function of Fe content. In the absence of water, H_2S uptake decreases with increasing Fe content from 5 to 10 mol%, whereas no further decrease is observed at the level of 15 mol% Fe. In contrast, the presence of 1 vol% H_2O in the feed stream leads to 21% more H_2S uptake for the solids containing 5 mol% Fe and 38% more H_2S uptake for the solids containing 10 mol% Fe. However, for the solid with 15 mol% Fe content, the presence of 1 vol% H_2O leads to a significantly lower H_2S uptake (a 42% decrease).

The simplest reaction scheme consistent with these observations is the following (the case of a $M^{II}O$ metal oxide):

$$H_2S + MO \Leftrightarrow MS + H_2O, \quad (3)$$

$$H_2O + MO \Leftrightarrow M(OH)_2, \quad (4)$$

$$H_2S + M(OH)_2 \Leftrightarrow MS + 2H_2O. \quad (5)$$

According to reactions (3)–(5), the presence of water can cause hydroxylation of the oxidic surface and of the bulk of the oxide (subsurface region). In the case of ZnO, the hydroxylated surface resulted in higher rates for H_2S adsorption and surface

diffusion of the derived species [45]. It was also reported [19] that a water-promoted cation diffusion mechanism operated in the case of interaction of H_2S (0.05–0.8% in N_2) with ZnO at 45 °C facilitated the formation of ZnS.

Fig. 11b presents the effect of H_2O feed concentration (1–3 vol%) on H_2S uptake for the 5 Fe–15 Mn–40 Zn–40 Ti–O solid as a function of adsorption temperature. The presence of 1 vol% H_2O in the feed results in lower H_2S uptakes in the 75–100 °C range, where the beneficial effect of H_2O in the sulfidation process (promotion of the cation diffusion mechanism [5]) is significantly reduced. In contrast, at 25 °C, a 20% increase in H_2S uptake is observed due to the water-induced promotion of cation diffusion mechanism. It is likely that formation of a metal hydroxide shell to a greater extent at 75–100 °C than at 25 °C limits diffusion of HS^- and S^{2-} into the bulk of unreacted oxide, thus reducing the final H_2S uptake.

Increasing the water feed concentration to the level of 3 vol%, produces a different profile for the H_2S–temperature relationship. In the 75–100 °C range, H_2S uptake increases significantly with respect to the case of 1 vol% H_2O in the feed stream. But at 25 °C, the presence of 3 vol% H_2O in the feed leads to lower H_2S uptake compared with the case of 1 vol% H_2O. It seems that H_2O promotes the cation diffusion mechanism in the 75–100 °C range but not at 25 °C. These results suggest a different mechanism of sulfidation propagation by increasing the water concentration in the feed stream. It is proposed that increasing the H_2O feed concentration increases the extent of surface hydroxylation. This different sulfidation mechanism is also supported by the different profile of H_2S uptake versus adsorption temperature in the case of 1 and 3 vol% H_2O. In the case of 1 vol% H_2O, H_2S uptake decreases as the temperature increases; the opposite is true in the case of 3 vol% H_2O. In both cases, a competitive adsorption of H_2O and H_2S must be proposed, and the overall process of sulfidation seems to be kinetically controlled.

3.2.5.2. Comparison with a Ni-based commercial adsorbent

Fig. 12 presents comparative results of the effect of temperature on H_2S uptake for the fresh sol–gel-prepared 5 Fe–15 Mn–40 Zn–40 Ti–O solid and the commercial Ni-based one in the presence of 1 vol% (Fig. 12a) and 3 vol% (Fig. 12b) water in the feed stream. In the presence of 1 vol% H_2O, the commercial catalyst appears to be superior to the sol–gel-prepared mixed-metal oxide in the 25–100 °C range. For the commercial adsorbent, H_2S uptake increases by 141% with an increase in adsorption temperature from 25 to 100 °C. In contrast, a 28% decrease in H_2S uptake is observed in the 5 Fe–15 Mn–40 Zn–40 Ti–O solid. In the case of 3 vol% H_2O in the feed stream, the sol–gel-prepared mixed-metal oxide is superior to the commercial one in the 25–75 °C range, but the commercial solid has a greater H_2S uptake at 100 °C.

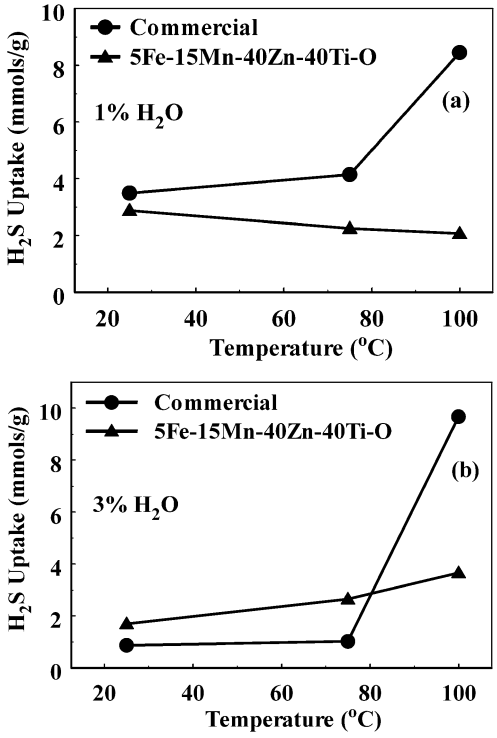

Fig. 12. Effect of 1 vol% H_2O (a) and 3 vol% H_2O (b) present in the adsorption gas mixture on the H_2S uptake (mmol/g) for the 5 Fe–15 Mn–40 Zn–40 Ti–O and Ni-based commercial solid adsorbents. Adsorption conditions: 0.06% H_2S/25% H_2/7.5% CO_2/x% H_2O/He, $x = 1$, 3 vol%; $F = 30$ NmL/min.

4. Conclusions

The following conclusions can be derived from the results of the present work:

1. The molar ratio of Fe/Mn used in the sol–gel synthesis of Fe–Mn–Zn–Ti–O mixed-metal oxides largely determines the morphology and the size of the solid particles formed. The morphology of 5 Fe–15 Mn–40 Zn–40 Ti–O and 20 Fe–40 Zn–40 Ti–O solids drastically changes after treatment of the solid with 0.06% H_2S/25% H_2/7.5% CO_2/He gas mixture (sulfidation) followed by regeneration in 20% O_2/He at 750 °C for 10 h.
2. The Fe/Mn molar ratio regulates the reducibility of Fe–Mn–Zn–Ti–O solids and possibly their reduction mechanism by hydrogen.
3. Raman and Mössbauer studies reveal that the presence of Mn in the 5 Fe–15 Mn–40 Zn–40 Ti–O solid makes the mixed oxide structures ($(Mn,Zn)Fe_2O_4$, $ZnMnO_3$) more susceptible to structural distortions during sulfidation and regeneration procedures.
4. According to the XPS results, migration of Fe ions through inner (during sulfidation) and outer (during regeneration) layers of the solid particles of 5 Fe–15 Mn–40 Zn–40 Ti–O is facilitated by the presence of Mn. A more detailed study for the intrinsic effect of Fe/Mn molar ratio on the cation migration mechanism is needed.
5. The lower H_2S uptake obtained on the 5 Fe–15 Mn–40 Zn–40 Ti–O solid after regeneration compared with the fresh one is due in part to the presence of remaining sulfates (SO_4^{2-}) and sulfides (S^{2-}) in the lattice, the formation of which is favored in the presence of Mn. The lowest percentage regeneration is obtained after exposure of the fresh solids to the H_2S-containing gas mixture at 25 °C and

regenerated at 750 °C, whereas the highest percentage regeneration is obtained when regeneration is conducted at 500 °C.

6. The sol–gel-prepared 5 Fe–15 Mn–40 Zn–40 Ti–O solid shows a significantly greater (by a factor of 3.2) H_2S uptake than the commercial Ni-based adsorbent at an adsorption temperature of 25 °C and similar uptake at 50 °C. However, at 75 and 100 °C the commercial adsorbent exhibits greater H_2S uptake (by a factor of 2.2 and 1.9, respectively).
7. The presence of 1–3 vol% H_2O in the 0.06% H_2S/25% H_2/7.5% CO_2/He gas mixture significantly enhances H_2S uptake at 25 °C for the 5 Fe–15 Mn–40 Zn–40 Ti–O solid. The presence of 3 vol% H_2O seems to alter the sulfidation mechanism of the solid.
8. The fundamental knowledge derived from this study on the chemical interaction of H_2S with the newly developed Fe–Mn–Zn–Ti–O mixed-metal oxide materials and also that of air with the sulfated materials can be used to drive further investigations into these new, more environmentally friendly materials for use in the important industrial catalytic oxidation of H_2S to elemental sulfur.

Acknowledgments

Financial support from the European Union (5th FP) through the EVK1-CT-1999-00033 research project and of the Research Committee of the University of Cyprus is gratefully acknowledged. The research group of Professor P.G. Koutsoukos at the Chemical Engineering Department of the University of Patras (Greece) is also acknowledged for the SEM measurements.

References

[1] J. Wieckowska, Catal. Today 24 (1995) 405.
[2] L. Saleta, Chem. Prum. 25 (1975) 2.
[3] M. Stejins, P. Mars, Ind. Eng. Chem. Prod. Res. Dev. 16 (1977) 35.
[4] J.B. Hyne, Oil Gas J. 70 (1972) 64.
[5] D. Stirling, The Sulfur Problem: Cleaning up Industrial Feedstocks, The Royal Society of Chemistry, London, 2000.
[6] S. Ozdemir, T. Bardakci, Sep. Purif. Technol. 16 (1999) 225.
[7] M. Hartman, R. Coughlin, AIChE J. 22 (3) (1976) 490.
[8] R. Ayala, W. Marsh, Ind. Eng. Chem. Res. 30 (1991) 55.
[9] S. Lew, K. Jothimurugesan, M.F. Stephanopoulos, Chem. Eng. Sci. 47 (1992) 1421.
[10] M.C. Woods, S.K. Gangwal, D.P. Harrison, K. Jothimurugesan, Ind. Eng. Chem. Res. 30 (1991) 100.
[11] F.A. Jale, A. Ates, Gas Sep. Purif. 9 (1995) 17.
[12] S.S. Tamhankar, M. Bagajenicz, G.R. Gavalas, S.M. Flytzani, Ind. Eng. Chem. Process Des. Dev. 25 (1986) 429.
[13] S.M. Flytzani, R.G. Gavalas, S.S. Tamhankar, US Pat. 4729889 (1989).
[14] P.V. Focht, G.D. Ranade, D.P. Harrison, Chem. Eng. Sci. 48 (11) (1988) 3005.
[15] T. Grindley, G. Steinfeld, DOE/MC/16545-1125 (1981).
[16] H. Kobayashi, M. Shirai, M. Nunokawa, Energy Fuels 11 (1997) 887.
[17] H. Kobayashi, M. Shirai, M. Nunokawa, Energy Fuels 16 (2002) 601.
[18] T. Baird, P.J. Denny, R.W. Hoyle, F. McMonagle, D. Stirling, J. Tweedy, J. Chem. Soc., Faraday Trans. 88 (22) (1992) 3375.
[19] J.M. Davidson, C.H. Lawrie, K. Sohail, Ind. Eng. Chem. Res. 34 (9) (1995) 2981.
[20] T. Baird, K.C. Campbell, P.J. Holliman, R.W. Hoyle, D. Stirling, B.P. Williams, J. Mater. Chem. 7 (2) (1997) 319.
[21] T. Baird, K.C. Campbell, P.J. Holliman, R.W. Hoyle, M. Huxam, B.P. Stirling, D. Williams, M. Morris, J. Mater. Chem. 9 (2) (1999) 599.
[22] C.L. Carnes, K.J. Klabunde, Chem. Mater. 14 (2002) 1806.
[23] E. Sasaoka, S. Hirano, S. Kasasoka, Y. Sakata, Energy Fuels 8 (1994) 1100.
[24] T. Baird, K.C. Campbell, P.J. Holliman, R. Hoyle, D. Stirling, B.P. Williams, J. Chem. Soc., Faraday Trans. 92 (3) (1996) 445.
[25] T. Baird, K.C. Campbell, P.J. Holliman, R.W. Hoyle, D. Stirling, B.P. Williams, M. Morris, J. Chem. Soc., Faraday Trans. 91 (18) (1995) 3219.
[26] T.J. Bandosz, Carbon 37 (1999) 483.
[27] A. Bagreev, H. Rahman, T.J. Bandosz, Carbon 39 (2001) 1319.
[28] K. Polychronopoulou, J.L.G. Fierro, A.M. Efstathiou, Appl. Catal. B 57 (2004) 125.
[29] R.J.A.M. Terode, M.C. de Jong, M.J.D. Crombag, P.J. van de Brink, A.J. van Dillen, J.W. Geus, Stud. Surf. Sci. Catal. 82 (1994) 861.
[30] P.F.M.T. van Nisselrooy, J.A. Lagas, Catal. Today 16 (1993) 263.
[31] Z.M. George, Adv. Chem. Ser. 139 (1975) 75.
[32] M.A.B. Saad, O. Saur, Y. Wang, C.P. Tripp, B.A. Morrow, C.J. Lavalley, J. Phys. Chem. 99 (1995) 4620.
[33] A.A. Davydov, V.I. Marshneva, M.L. Shepotko, Appl. Catal. A: Gen. 244 (2003) 93.
[34] K.-T. Li, C.-S. Yen, N.-S. Shyu, Appl. Catal. A: Gen. 156 (1997) 117.
[35] European project (5th FP), EVK1-CT-1999-00033, Development of Technologies Using the Activity of Sulphate and Metal Reducing Bacteria (SMRB) to Remove Heavy Metals and Metalloids from Ground Waters and Soils.
[36] L.L. Hench, J.K. West, Chem. Rev. 90 (1990) 33.
[37] C.N. Costa, T.A. Anastasiadou, A.M. Efstathiou, J. Catal. 194 (2000) 250.
[38] E. Auzans, D. Zins, E. Blums, R. Massart, J. Mater. Sci. 34 (1999) 1253.
[39] J.F. Akyurtlu, A. Akyurtlu, Gas Sep. Purif. 9 (1995) 17.
[40] W. Kim, F. Saito, Powder Technol. 114 (2001) 12.
[41] M. Baldi, V.S. Escribano, J.M.G. Amores, F. Milella, G. Busca, Appl. Catal. B 17 (1998) L175.
[42] M.A. Ahmed, E. Garcia, L. Alonso, J.M. Palacios, Appl. Surf. Sci. 156 (2000) 115.
[43] G.A. Bukhtiyarova, V.I. Bukhtiyarov, N.S. Sakaeva, V.V. Kaichev, B.P. Zolotovskii, J. Mol. Catal. 158 (2000) 251.
[44] I.I. Novochinskii, C. Song, X. Ma, X. Liu, L. Shore, J. Lampert, R.J. Farrauto, Energy Fuels 18 (2004) 576.
[45] C.H. Lawrie, Ph.D. Thesis, University of Edinburgh, Edinburgh, 1990.
[46] R.V. Siriwardane, J.A. Poston, G. Evans, Ind. Eng. Chem. Res. 33 (1994) 2810.
[47] B. Gillot, M.El. Guendouzi, M. Laarj, Mater. Chem. Phys. 70 (2001) 54.
[48] B. Gillot, J. Solid State Chem. 113 (1994) 163.
[49] M.A. Ahmed, L. Alonso, J.M. Palacios, C. Cilleruelo, J.C. Abanades, Solid State Ionics 138 (2000) 51.
[50] H.-Y. Lin, Y.-W. Chen, C. Li, Thermochim. Acta 400 (2003) 61.
[51] M.A. Peña, J.L.G. Fierro, Chem. Rev. 101 (2001) 1981.
[52] J.W. Niemantsverdriet, Spectroscopy in Catalysis, VCH, Weinhein, 1993.
[53] M. Ziolek, I. Sobczak, I. Nowak, M. Daturi, J.C. Lavalley, Top. Catal. 11/12 (2000) 343.
[54] M. Ziolek, J. Kujawa, O. Saur, J.C. Lavalley, J. Mol. Catal. A 97 (1995) 49.
[55] A. Travert, O.V. Manoilova, A.A. Tsyganenko, F. Mauge, J.C. Lavalley, J. Phys. Chem. B 106 (2002) 1350.
[56] J.A. Poston, Ind. Eng. Chem. Res. 35 (1996) 875.
[57] H.W. Nesbitt, G.M. Bancroft, A.R. Pratt, M.J. Scaini, Am. Miner. 83 (1998) 1067.
[58] F.A. Al-Sagheer, M.I. Zaki, Colloids Surf. A 173 (2000) 193.
[59] J.E. Thomas, C.F. Jones, W.M. Skinner, R.St.C. Smart, Geochim. Cosmochim. Acta 62 (9) (1998) 1555.
[60] J. Wang, C. Zeng, Z. Peng, Q. Chen, Physica B 349 (2004) 124.
[61] N.N. Greenwood, T.C. Gibb, Mössbauer Spectroscopy, Chapman and Hall Ltd., London, 1971, p. 284.
[62] Z.H. Zhou, J. Wang, J.M. Xue, H.S.O. Chan, J. Mater. Chem. 11 (2001) 3110.
[63] M.H. Sousa, F.A. Tourinho, J.C. Roubim, J. Raman Spectrosc. 31 (2000) 185.

[64] O. Yamashita, T. Ikeda, J. Appl. Phys. 95 (2004) 1743.
[65] S.B. Turcotte, R.E. Benner, A.M. Riley, J. Li, M.E. Wadsworth, Appl. Optics 32 (1993) 935.
[66] J.R. Mycroft, G.M. Bancroft, N.S. McIntyre, J.W. Lorimer, I.R. Hill, J. Electroanal. Chem. 292 (1990) 139.
[67] R. Woods, D.C. Constable, I.C. Hamilton, Int. J. Miner. Process 27 (1989) 309.
[68] M.V. Abrashev, J. Backstrom, L. Borjesson, Phys. Rev. B 64 (2001) 144429.
[69] E. Liarokapis, Th. Leventouri, D. Lampakis, D. Palles, J.J. Neumeier, D.H. Goodwin, Phys. Rev. B 60 (1999) 758.
[70] V. Dediu, C. Ferdeghini, F.C. Matacotta, P. Nozar, G. Ruani, Phys. Rev. Lett. 84 (2000) 4489.
[71] E. Granado, J.A. Sanjurjo, C. Rettori, J.J. Neumeier, S.B. Oseroff, Phys. Rev. B 62 (2000) 11304.
[72] M.V. Abrashev, A.P. Litvinchuk, M.N. Iliev, R.L. Meng, V.N. Popov, V.G. Ilanov, R.A. Chakalov, C. Thomsen, Phys. Rev. B 59 (1999) 4146.
[73] E. Granado, N.O. Moreno, A. Garcia, J.A. Sanjurjo, C. Rettori, I. Torriani, S.B. Oseroff, J.J. Neumeier, Phys. Rev. B 58 (1998) 11435.
[74] K.D. Cleaver, J.E.D. Davies, J. Raman Spectrosc. 9 (1980) 376.
[75] P.D. Clark, N.I. Dowling, M. Huang, O. Okemona, G.D. Butlin, R. Hou, W.S. Kijlstra, Appl. Catal. A: Gen. 235 (2002) 61.
[76] S. Lew, K. Jothimurugesan, M. Flytzani-Stephanopoulos, Ind. Eng. Chem. Res. 28 (1989) 535.
[77] R.B. Slimane, J. Abbasian, Adv. Environ. Res. 4 (2000) 147.